Lithos 256–257 (2016) 165–181

Contents lists available at ScienceDirect

Lithos

journal homepage: www.elsevier.com/locate/lithos

High-alumina basalts from the Bogda Mountains suggest an arc setting for Chinese Northern Tianshan during the Late Carboniferous

Wei Xie [a], Yi-Gang Xu [a,*], Yi-Bing Chen [a], Zhen-Yu Luo [a], Lu-Bing Hong [a], Liang Ma [a], Hai-Quan Liu [b]

[a] State Key Laboratory of Isotope Geochemistry, Guangzhou Institute of Geochemistry, Chinese Academy of Sciences, Guangzhou 510640, PR China
[b] Key Laboratory of Marginal Sea Geology, Guangzhou Institute of Geochemistry, Chinese Academy of Sciences, Guangzhou 510640, PR China

ARTICLE INFO

Article history:
Received 1 January 2016
Accepted 5 April 2016
Available online 13 April 2016

Keywords:
High-alumina basalt
Bogda Mountains
Arc setting
Late Carboniferous
Chinese Northern Tianshan

ABSTRACT

Considerable debate persists as to the tectonic setting of the Tianshan Orogen during the Late Paleozoic, with active subduction system and intraplate large igneous provinces as two dominant schools. With aims of providing constraints on this issue, geochronological and geochemical analyses have been carried out on the Late Carboniferous high-Al basaltic lava (HAB) from the Bogda Mountains. These lavas, in conformable contact with the felsic rocks, belong to the Upper Carboniferous Liushugou Group. Zircon SHRIMP U–Pb dating of two felsic ignimbrites further suggest that they were mainly erupted during 315–319 Ma. The Bogda basaltic lava is classified as HAB given their high Al contents >16% and their chemical resemblance to those from modern arcs such as Aleutian and Kamchatka. They are characterized by strong enrichment in large ion lithophile elements (LILE), strong negative Nb–Ta and Ti anomalies, and distinct positive Pb anomalies. Hence, they are significantly different from the mantle plume-related basalts, as exemplified by those from Siberian, Emeishan, and Tarim large igneous provinces. Instead, their MORB-like Nd–Hf–Pb isotopes and arc-like trace elements indicate that the Bogda HABs may have been generated from a mantle wedge metasomatized by sediment-derived melts. The sector and oscillatory zoning in clinopyroxene phenocrysts in the Bogda HABs is attributable to rapid dynamic crystallization during magma ascent. High Al content is due to delayed plagioclase nucleation likely by the high crystallization pressure rather than water content. Collectively, our data lend support to an island arc environment during the Late Paleozoic, probably related to southward subduction of the Paleo-Tianshan Ocean.

1. Introduction

The Chinese Northern Tianshan is a key area for understanding the Paleozoic tectonics and long-lasting evolution of the Central Asian Orogenic Belt (CAOB; Sengör et al., 1993; Wilhem et al., 2012; Windley et al., 2007; W.-J. Xiao et al., 2004; Xiao et al., 2013). The E–W trending Bogda–Harlik (B–H) belt, occurring exclusively in the northern part of the Chinese North Tianshan, is an important tectonic belt separating the Juggar Basin to the north and the Tu–Ha Basin to the south (Fig. 1A). The key issues surrounding the B–H belt include 1) its tectonic nature in the Late Paleozoic and 2) the timing of final closure of the Paleo-Tianshan Ocean. Some researchers suggested that the Paleo-Tianshan Ocean closed by the end of Early Paleozoic (He et al., 1994) or Devonian (Xia et al., 2008, 2012). Accordingly, most part of the Carboniferous and Permian saw an intraplate setting, and the volcanic rocks erupted during this period may reflect responses to continental rifting (Che et al., 1996; Gu et al., 2000, 2001) or represent a large igneous province associated with a mantle plume (Xia et al., 2004, 2008, 2012). Others believed that it closed during the Late Carboniferous (Gao et al., 1998; Shu et al., 2011; Windley et al., 1990). This derives from the idea of a Carboniferous island arc setting to Permian post-collisional orogenic setting (Chen et al., 2011; Laurent-Charvet et al., 2003; Ma et al., 1997; Shu et al., 2011; W.-J. Xiao et al., 2004; Yuan et al., 2010; Zhu et al., 2009). Otherwise, some also argued that the Paleo-Tianshan Ocean closed at the end of Early Carboniferous given the occurrence of ~316 Ma A-type "stitching pluton" (Chen et al., 2011; Han et al., 2010).

Magmatism provides a clue to evaluate these competing models. Late Carboniferous–Permian volcano-sedimentary rocks are widely exposed in the Bogda Mountains, consisting of basaltic and rhyolite lava, felsic ignimbrite, breccia, and volcanic clastic sedimentary rocks (Fig. 1B; BGMRXUAR, 1993; Gu et al., 2001; Liang et al., 2011; Zhao et al., 2014). Among these volcanic rocks, high-Al basalt and basaltic andesite (HAB) are particularly interesting, because these rock types are generally associated with arcs or mid-ocean ridges on a global scale (e.g., Crawford et al., 1987; Eason and Sinton, 2006; Grove et al., 1988; Kuno, 1960; Ozerov, 2000; Sisson and Grove, 1993a).

Pioneering work by Tilley (1950) recognized HAB as a new magma type. Kuno (1960) reported the existence of three different primary magma types in the Japan arc (tholeiite, aphyric HAB, and alkali olivine

* Corresponding author at: State Key Laboratory of Isotope Geochemistry, Guangzhou Institute of Geochemistry, Chinese Academy of Sciences, 510640 Wushan, Guangzhou, PR China. Tel.: +86 20 85290109; fax: +86 20 85290261.
E-mail address: yigangxu@gig.ac.cn (Y.-G. Xu).

http://dx.doi.org/10.1016/j.lithos.2016.04.005
0024-4937/

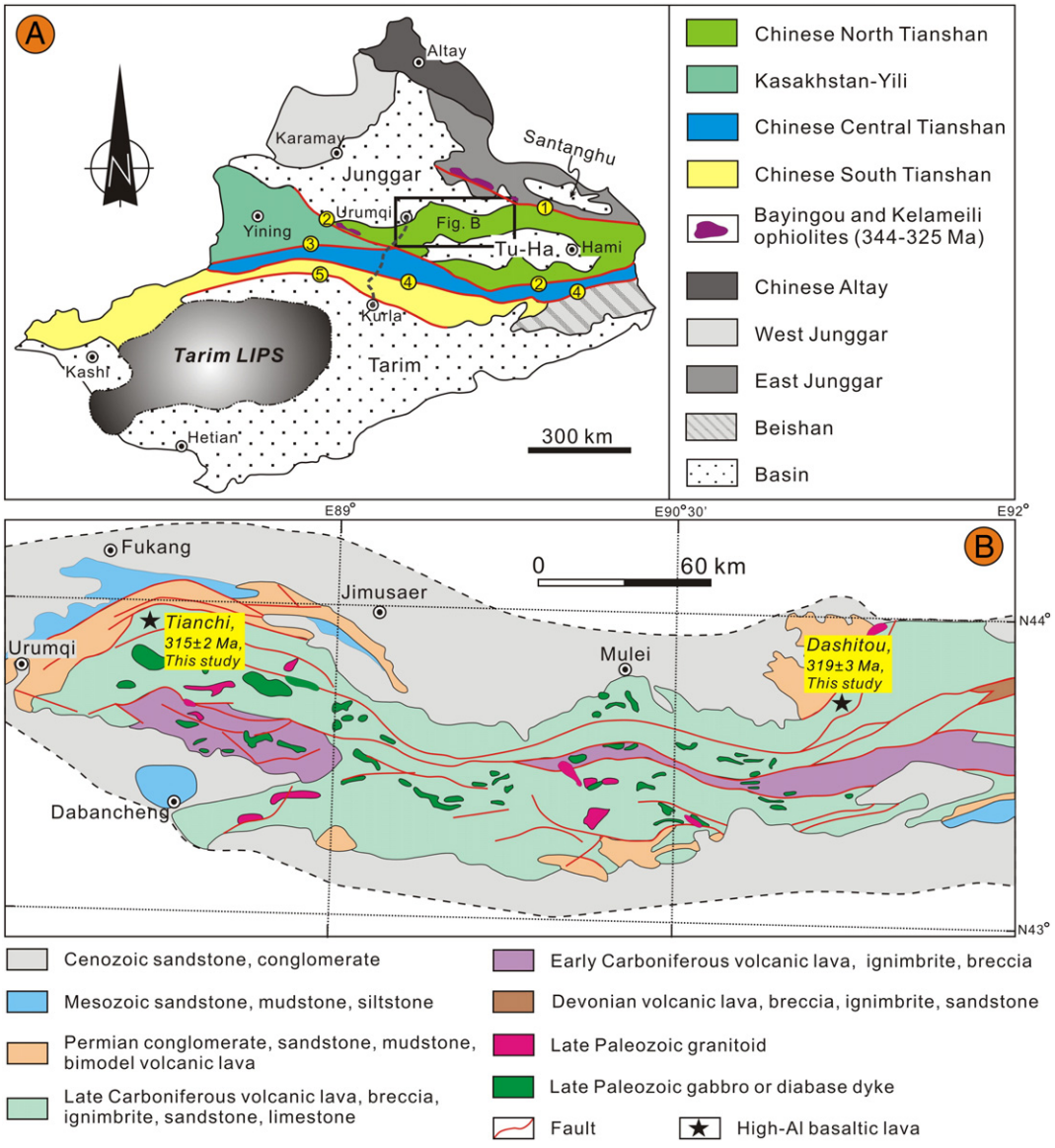

Fig. 1. A) Simplified tectonic sketch map of most part of Xinjiang province, NW China, modified after Pirajno et al. (2008), Wang et al. (2011), and Xiao et al. (2013), ① Kalameili Fault, ② North Tianshan–Aqikuduke–Shaquanzi Fault, ③ South Tianshan Future, ④ Kumishi–Kawabulake–Xingxingxia Fault, ⑤ North Tarim Suture; B) Geological map of the Bogda oregenic belt at the north margin of the Chinese North Tianshan, modified after Chen et al. (2011) and Zhao et al. (2014).

basalt). Subsequent research used "high-alumina basalt (HAB)" to refer to any sub-alkaline aphyric as well as porphyritic basaltic rock with Al_2O_3 > 16% (e.g., Crawford et al., 1987; Eason and Sinton, 2006; Ozerov, 2000; Sisson and Grove, 1993a). According to samples and experimental investigations, some workers further suggested that a slightly hydrous HAB (H_2O < 2%) always was tholeiite with olivine + high-CaO pyroxene + plagioclase + magnetite (late crystallization) mineral assemblages, whereas a wet HAB (H_2O > 2%) generally was calc-alkaline with olivine + high-CaO plagioclase + magnetite (early crystallization) + pyroxene/hornblende (Crawford et al., 1987; Hamada and Fujii, 2008; Sisson and Grove, 1993a, 1993b and references therein). Although some authors thought that the HAB might be generated by very high-degree partial melting of subducted oceanic slab (Brophy and Marsh, 1986; Johnson, 1986; Marsh, 1979, 1982), now most of researchers believe that it is likely generated by low-degree partial melting of mantle peridotite (Bartels et al., 1991; Crawford et al., 1987; Eason and Sinton, 2006; Green et al., 1967; Ozerov, 2000; Sisson and Grove, 1993a). The key factor for the genesis of high alumina may be due to the delayed plagioclase nucleation (Ariskin, 1999; Brophy, 1989; Crawford et al., 1987; Eason and Sinton, 2006; Green et al., 1967; Ozerov, 2000; Sisson and Grove, 1993a, 1993b), and/or preferential accumulation or flotation of plagioclase (Crawford et al., 1987; Yoder and Tilley, 1962). Furthermore, many workers believe that water (H_2O > 2%) plays a dominate role for the delayed plagioclase nucleation (Ariskin, 1999; Beard and Lofgren, 1992; Grove et al., 2012; Sisson and Grove, 1993a, 1993b). Nevertheless, others proposed that high pressure can also suppress plagioclase fractionation (Bartels et al., 1991; Crawford et al., 1987; Draper and Johnston, 1992; Eason and Sinton, 2006; Grove et al., 1982).

In this paper, we present SHRIMP U–Pb ages and geochemistry for the Late Carboniferous HAB from the Bogda belt. We compare the Bogda basalts with HABs from modern arcs and typical mantle plume-related basalts. Then we combine mineral geochemistry to constrain the petrogenesis of these rocks. Our results suggest that the Bogda HABs represent magmas formed in a Late Carboniferous island arc system. Here, we also emphasize that high pressure rather than water content plays a dominate role to delay plagioclase nucleation in a tholeiite HAB.

2. Regional geology

The Chinese Tianshan is a complex collage of island arc assemblages, remnants of oceanic crust, continental fragments and margins. It was formed by multiple subduction–accretion and collision processes from the Neoproterozoic to the Late Paleozoic, and then experienced Mesozoic thermal subsidence and Cenozoic thrusting and uplifts (Allen et al., 1993; Sengör et al., 1993; Windley et al., 1990, 2007; W.-J. Xiao et al., 2004; Xiao et al., 2013). The Chinese Tianshan can be generally subdivided into three geological units from south to north, separated by the Northern Tianshan–Aqikuduke–Shaquanzi Fault and the Kumishi–Kawabulake–Xingxingxia Fault: the Chinese North, Central and South Tianshan (Fig. 1A). Geographically, it can be also subdivided into western and eastern Tianshan by a boundary roughly along the Urumqi–Kurle road.

The Bogda–Harlik (B–H) belt encloses the northern part of the Chinese North Tianshan and contains Late Paleozoic to Quaternary sedimentary and igneous rocks. Nearby the B–H belt, the Kelameili and Bayingou ophiolites crop out mainly along the Kelameili fault in the Eastern Junggar and the Northern Tianshan fault, respectively (Fig. 1A). Jian et al. (2005) reported SHRIMP U–Pb ages of 497 ± 12 Ma and 403 ± 9 Ma for plagiogranite within the Kelameili ophiolites, while younger age (330 ± 2 Ma) for gabbro within the Kelameili ophiolites have been obtained by Wang et al. (2009). The geochemistry of the ophiolite suggests a supra-subduction zone (SSZ) origin in a forearc setting (Wang et al., 2003; Yang et al., 2009). Xu et al. (2006a, 2006b) reported a LA-ICP-MS U–Pb age of the gabbro (344 ± 3 Ma) and a SHRIMP U–Pb age of the plagiogranite (325 ± 7 Ma) for the Bayingou ophiolites. These two ophiolites are therefore the youngest ophiolites in the Chinese Tianshan, probably representing remnants of the Paleo-Tianshan Ocean (Han et al., 2010; Xiao et al., 2004b, 2008). The B–H belt was considered to be a Devonian to Carboniferous island arc system, resulting from the consumption of the Paleo-Tianshan Ocean (Han et al., 2010; W.-J. Xiao et al., 2004; Xiao et al., 2008; Yuan et al., 2010). The Bogda belt, which is the focus of this study, is the western part of the B–H belt (Fig. 1B).

The Devonian strata in the Bogda belt are dominated by marine–terrigenous tuffaceous sandstone and volcanic rock. The Carboniferous strata are in fault contact with the Devonian rocks and comprise three formations, namely, the Lower Carboniferous Qijiaojing Formation, the Upper Carboniferous Liushugou and Qijiagou Formations (BGMRXUAR, 1993; Gu et al., 2001; Liang et al., 2011; Xia et al., 2004; Zhao et al., 2014). The Lower and Upper Carboniferous Formations are separated by faults (Fig. 1B). The Lower Carboniferous Formation consists mainly of marine volcanic ignimbrite, tuffaceous sandstone, bimodal volcanic lava, while the Upper Carboniferous Formation is dominated by large volumes of shallow-marine (pillow) basaltic and rhyolite lava, felsic ignimbrite, with minor sandstone and siltstone. The Permian strata unconformably overlie the Carboniferous rocks. In this region, the Permian Formation is composed of terrestrial conglomerate, sandstone, siliceous mudstone intercalated with bimodal volcanic lava. Jurassic clastic sediment occurs in the southeast of the study area and lies unconformably over the Permian strata (Fig. 1B; BGMRXUAR, 1993; Carroll et al., 1990).

3. Petrology of the Bogda Late Carboniferous HAB

Two stratigraphic cross-sections of ~1000 m thick in the northern Bogda belt, i.e., the Tianchi and Dashitou sections, have been investigated (Fig. 1B). They comprise the Upper Carboniferous Liushugou Formation (BGMRXUAR, 1993; Gu et al., 2001; Liang et al., 2011; Xia et al., 2004) which is mainly composed of HAB, rhyolite lava, felsic ignimbrite and volcanic breccia (Fig. 2). The felsic ignimbrite is about 500 m thick and is trachyte and trachy-andesite. The rhyolite lava is about 30 m thick. Two layers of HABs are interlayered with the felsic rocks (Fig. 3A, B, C). One layer is ~100 m thick and the other is <10 m. In the Liushugou Formation, the volume ratio of the HAB against the felsic rocks is about 1: 6.

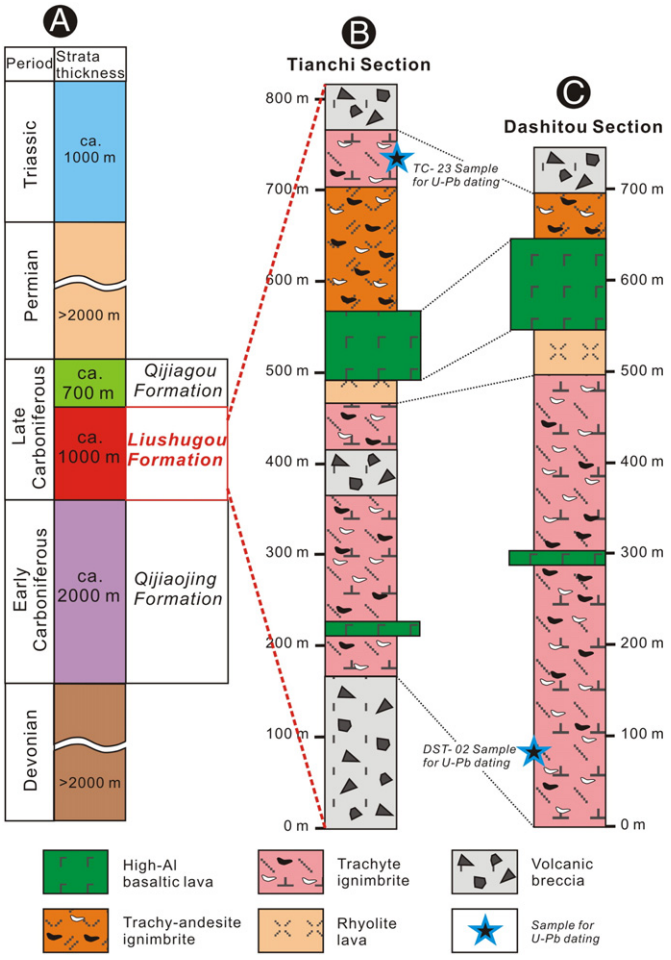

Fig. 2. (A) Simplified stratigraphy column from Devinian to Triassic in the Bogda area (modified after BGMRXUAR, 1993). (B, C) Two composite stratigraphy columns in Bogda area, showing the relationship of the high-Al basaltic lavas (HAB) and felsic rocks. The locations of the Tianchi and Dashitou geological cross-sections are shown in Fig. 1B.

The Bogda HABs can be further divided into two sub-groups: aphyric and porphyritic basalts. The aphyric HAB is high-MgO (see geochemistry section below), contain tiny mafic minerals, plagioclase, and Fe–Ti oxides (Fig. 3E). In contrast, the porphyritic HAB is low-MgO HAB, showing porphyritic texture and contains 5–25% phenocryst and 75–95% matrix (Fig. 3F). The phenocrysts are mainly clinopyroxene and plagioclase with minor magnetite. Their matrix is composed of mafic minerals, plagioclase, and Fe–Ti oxides. Clinopyroxene phenocrysts are more euhedral and bigger in size than plagioclase and magnetite, suggesting that clinopyroxene crystallized earlier than the other two minerals. Some phenocrysts suffered late hydrothermal alteration to chlorite and sericite. Many clinopyroxene phenocrysts show sector and oscillatory zoning (Fig. 9). Significantly, no olivine or hydrous minerals (e.g., biotite and hornblende) are found in the Bogda HABs (Fig. 3).

4. Analytical methods

4.1. Zircon U–Pb dating

Approximately 5 kg of each trachyte ignimbrite (DST-02 and TC-23) was crushed for zircon separation. Zircons were concentrated using conventional magnetic and heavy liquid separation methods, and then handpicked out under a binocular microscope. Selected zircon grains were mounted in epoxy resin along with chips of the zircon standard

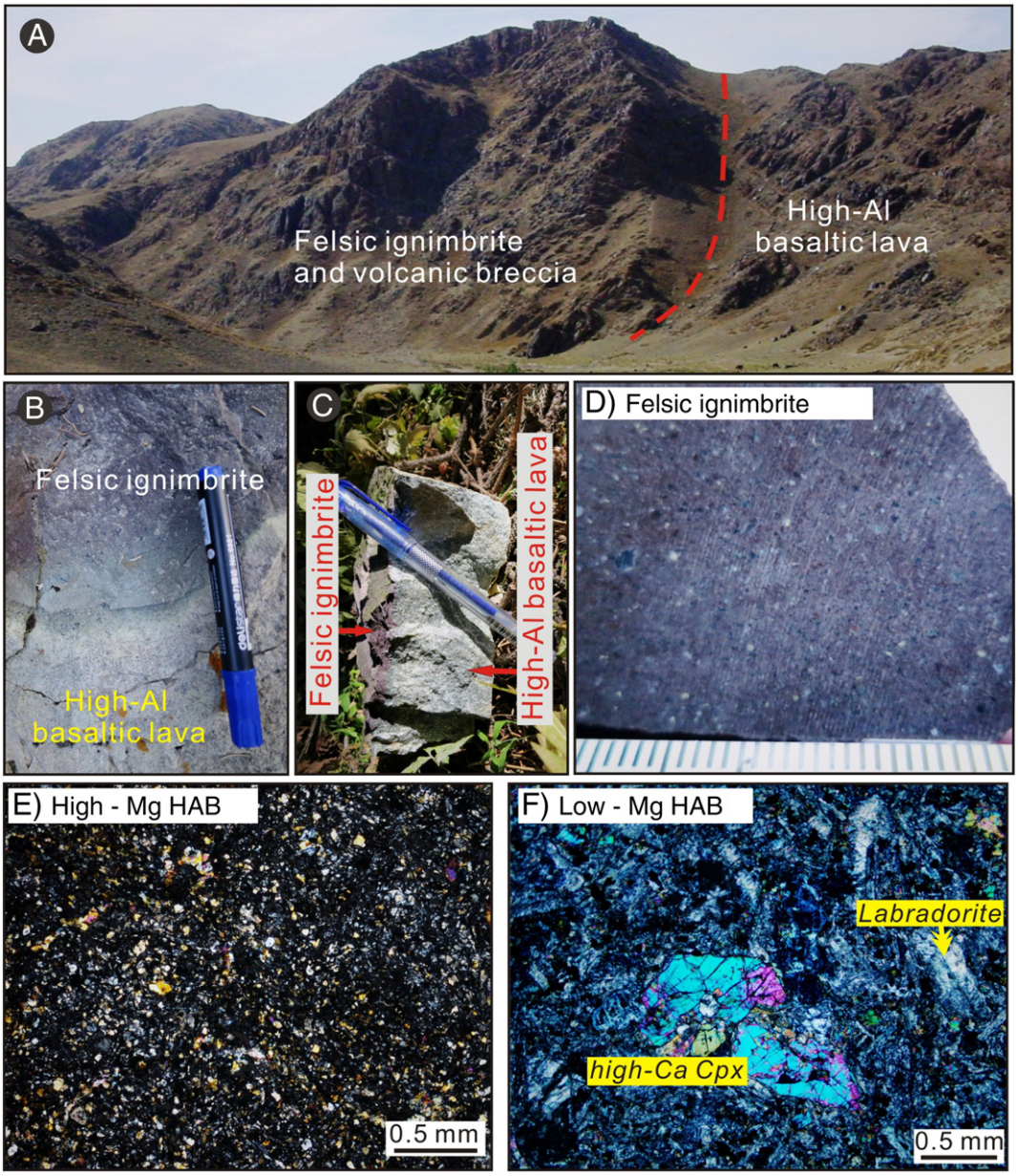

Fig. 3. (A, B, C) Field photos showing the conformable contacts between the Bogda HAB and felsic rocks. (D) Hand sample of the felsic ignimbrites for U–Pb dating. (E, F) Photomicrographs of the Bogda high-Al basalt (HAB). High-Ca Cpx = high-Ca clinopyroxene; Mt. = magnetite; Chl = chlorite.

TEMORA 1 (417 Ma; Black et al., 2003), and then polished before they were vacuum-coated with high purity gold.

The cathodoluminescence (CL) images were taken using a HITACHI S3000-N scanning electron microscope (SEM) and in situ zircon U–Th–Pb analyses were performed on a SHRIMP-II instrument at Curtin University, Western Australia. The instrument was controlled and data acquired using the SHRIMP Remote Operation System (SROS) from a remote control center in the Beijing SHRIMP Center, Institute of Geology, CAGS, Beijing. Analytical procedures follow those of Compston et al. (1992) and Williams (1998). Standard zircon sample SL 13 (572 Ma) was measured to calibrate U, Th, and Pb concentrations, and standard zircon TEMORA 1 were used for the isotopic fractionation correction. Common Pb correction was made using the ^{204}Pb-based method. Data processing was carried out using the SQUID 1.03 and Isoplot/Ex2.49 programs of Ludwig (2001a, 2001b). Uncertainties for each analysis are at 1σ, whereas the weighted mean age is quoted at 2σ. The analytical data are presented in Appendix A1 and on Concordia plots in Fig. 4.

4.2. Major and trace elements

Nine relatively fresh basaltic samples were chosen for major and trace element analysis. 0.7 g powder of such samples was mixed completely with $Li_2B_4O_7$–$LiBO_2$ flux and then fused to a glass bead at 1050–1100 °C in an automatic melting instrument. Major element analyses were carried out using X-ray fluorescence spectrometry (XRF, Rigaku ZSX-100e) on fused glass beads at Guangzhou Institute of Geochemistry, Chinese Academy of Sciences (GIGCAS), following the analytical procedures described by Goto and Tatsumi (1996). Analytical uncertainties are mostly between 1 and 5%. Trace element concentrations were determined on a PerkinElmer Sciex ElAN 6000 ICP-MS, following the techniques described by Liu et al. (1996). The USGS and Chinese National standards AGV-2, BHVO-2, GSR-1, GSR-2, GSR-3, and W-2 were chosen for calibrating element concentrations of the analyzed samples. The analytical precision is better than 5% for elements >10 ppm, less than 8% for those <10 ppm, and about 10% for transition metals.

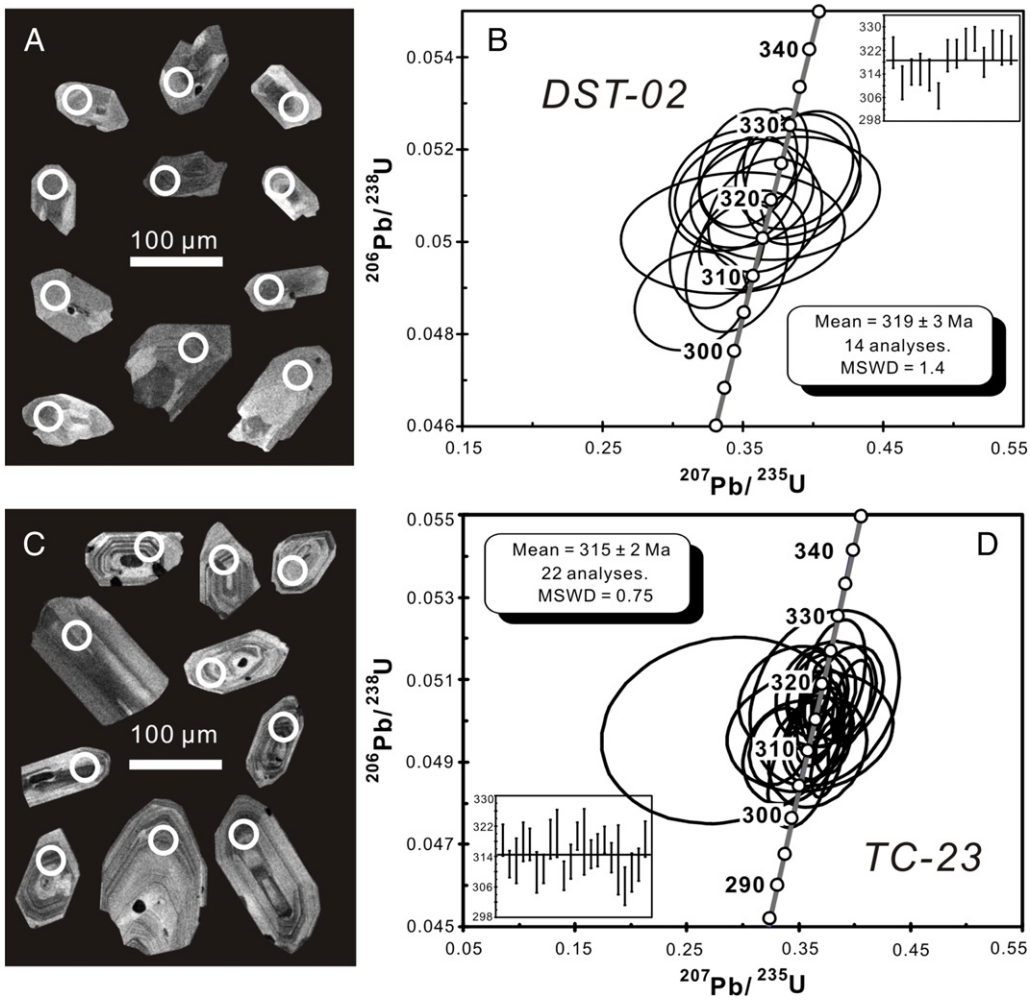

Fig. 4. CL images of representative zircons (A for DST-02 from the Dashitou section and C for TC-23 from the Tianchi section) and concordia plot of SHRIMP zircon U–Pb dating results for the trachyte ignimbrites (DST-02 and TC-23).

4.3. Nd, Hf, Pb isotopes

Whole rock Nd and Hf isotopic ratios were measured with a Micromass Isoprobe Multi-Collector ICP-MS at GIGCAS, using analytical procedures described by Li et al. (2006). The mass fractionation corrections for the isotopic ratios are based on $^{146}Nd/^{144}Nd = 0.7219$ and $^{179}Hf/^{177}Hf = 0.7325$, respectively. The reported $^{143}Nd/^{144}Nd$ and $^{176}Hf/^{177}Hf$ ratios were respectively adjusted to the Shin Etsu JNdi-1 standard $^{143}Nd/^{144}Nd = 0.512115$ and the JMC14374 standard $^{176}Hf/^{177}Hf = 0.282178$.

For whole rock Pb isotopic determinations, about 100 mg powder was weighed into a Teflon beaker, spiked and dissolved in concentrated HF at 180 °C for 7 h. Lead was separated and purified by conventional cation-exchange technique (AG1 × 8, 20–400 resin) with diluted HBr as an eluant. Total procedural blanks were <50 pg Pb. Isotopic ratios were measured by a VG-354 mass-spectrometer at the GIGCAS. Repeated analyses of SRM 981 yielded average values of $^{206}Pb/^{204}Pb = 16.9325 \pm 3$ (2σ), $^{207}Pb/^{204}Pb = 15.4853 \pm 3$ (2σ), and $^{208}Pb/^{204}Pb = 36.6780 \pm 9$ (2σ). External precisions are estimated to be less than 0.005, 0.005, and 0.0015.

4.4. Mineral chemistry

Four representative samples are selected to analyze the fresh pyroxene and plagioclase phenocrysts. Major element analysis and back-scattered electron (BSE) imaging of minerals were carried out using a JEOL JXA-8230 electron probe microanalyzer (EPMA) at the GIGCAS. The operating conditions are 15 kV accelerating voltage, 20 nA beam current, 1 μm beam diameter, and 20 s peak counting time for Si, Al, Fe, Mg, Ca (40 s for Ti, Mn; 60 s for Ni, Cr; 10 s for K, Na).

5. Analytical results

5.1. Zircon U–Pb age

The zircons (mostly <100 μm) from DST-02 exhibit transparent, stubby prismatic morphologies and fuzzy concentric oscillatory internal structures in CL. The zircons (mostly <200 μm) from TC-23 have similar morphologies but show distinct concentric oscillatory internal structures in CL. The zircons from DST-02 and TC-23 both show typical characteristics of igneous zircon and no inherited zircon cores are observed (Fig. 4A, C). The zircons from DST-02 have low U and Th contents of 70–256 ppm and 30–251 ppm, respectively, with Th/U ratios of 0.33–1.35 (Appendix A1). Fourteen analyses form a tight cluster on the Concordia plot and yield a weighted mean $^{206}U/^{238}Pb$ age of 319 ± 3 Ma (MSWD = 1.4) (Fig. 4B). Compared to DST-02, the zircons from TC-23 have relatively higher and scattered U and Th contents of 59–565 ppm and 33–709 ppm, respectively, with similar Th/U ratios of 0.47–1.3 (Appendix A1). Twenty-two analyses form a tight cluster on the Concordia plot and yield a weighted mean $^{206}U/^{238}Pb$ age of 315 ± 2 Ma (MSWD = 0.75) (Fig. 4D). The two zircon U–Pb ages are

concurrent within the error range and indicate that the volcanics from the Liushugou Formation were erupted during 315–319 Ma.

5.2. Major and trace elements

The Bogda HABs have LOI contents ranging from 2.3 to 5.2%, consistent with petrographic evidence for partial alteration. In the following plots and discussion, all oxide contents of the samples have been recalculated to 100% on a volatile-free basis with all Fe as FeO (Appendix A2).

The Bogda basaltic samples show scattered SiO_2 (48.8–56%) and alkali (2.7–5.8%) contents (Fig. 5A). As shown in Fig. 5D, they are similar to the high-Al basalt and basaltic andesite (HAB) defined by Kuno (1960). But they have higher alkali contents in comparison with modern HABs (i.e., the Aleutian, Izu, Japan, and Kamchatka Islands), probably due to Na_2O and K_2O mobility during alteration, in accordance with their high LOI contents. The Zr/TiO_2 versus Nb/Y diagram (Winchester and Floyd, 1977), therefore, is utilized for rock classification, because all the elements are considered to remain immobile during alteration/weathering. In Fig. 5B, the Bogda HABs fall in the field of andesite/basalt. They straddle the line separating tholeiite and calc-alkaline affinities (Fig. 5C), but most of them belong to tholeiite which are similar to the modern HABs. We also use tholeiitic index (THI = $Fe_{4.0}/Fe_{8.0}$; Zimmer et al., 2010) to characterize the studied samples, where $Fe_{4.0}$ is the average FeO_T concentration of samples with 4 ± 1 wt% MgO, and $Fe_{8.0}$ is the average FeO_T at 8 ± 1 wt% MgO. The calculated result shows that the THI of the Bogda HABs is 1.05, consistent with a tholeiitic affinity (THI > 1). Two Bogda samples have relatively high MgO (9.1–9.8%), Mg# (62–65), Cr (586–644 ppm), Ni (154–208 ppm), and Al_2O_3 (16.1–16.5%). Compared to these high-MgO samples, the other Bogda samples have lower MgO (3–7.5%), Mg# (41–61), Cr (<130 ppm), Ni (<60 ppm) but higher Al_2O_3 (16.4–19.1%).

The Bogda HABs show large ranges of total REEs (ΣREEs = 40–150 ppm), enrichment of LREEs over HREEs ($(La/Yb)_N$ = 2.0–5.7, $(Dy/Yb)_N$ = 1.2–1.4; Fig. 7A) and weak negative to positive Eu anomalies (δEu = 0.9–1.1). On the trace element spider diagrams, they are marked by strong enrichment in large ion lithophile elements (LILE) relative to high field strength elements (HFSE). Furthermore, they show negative Nb–Ta and Ti anomalies and distinct positive Pb anomalies, which are similar to arc basalts worldwide but are clearly distinct from ocean island basalts (OIB; Fig. 7B).

5.3. Nd, Hf, Pb isotopes

The measured isotope ratios were corrected to 315 Ma based on Sm, Nd, Lu, Hf, U, Th, and Pb concentrations determined by ICP-MS (Appendix A3). On the whole, the Bogda HABs have quite uniform $(^{143}Nd/^{144}Nd)_t$ of 0.51257–0.51261 ($\varepsilon_{Nd(t)}$ = 6.75–7.43) and $(^{176}Hf/^{177}Hf)_t$ of 0.28293–0.28299 ($\varepsilon_{Hf(t)}$ = 12.7–14.7). On the $\varepsilon_{Hf(t)}$ versus $\varepsilon_{Nd(t)}$ diagram, all samples plot between the MORB + OIB [$\varepsilon_{Hf(t)} = 1.59\varepsilon_{Nd(t)} + 1.28$] and Island Arc [$\varepsilon_{Hf(t)} = 1.23\varepsilon_{Nd(t)} + 6.36$] arrays of Chauvel et al. (2008, 2009) (Fig. 8A). They also have restricted $(^{206}Pb/^{204}Pb)_t$ (17.81–17.88), $(^{207}Pb/^{204}Pb)_t$ (15.46–15.48), and $(^{208}Pb/^{204}Pb)_t$ (37.47–37.65). Fig. 8 illustrates that the Bogda HABs have lower Pb isotopes relative to the Aleutian and Kamchatka HABs and are close to depleted mantle (DM).

5.4. Mineral compositions

Major element compositions of pyroxene phenocrysts from the Bogda low-MgO HABs are listed in Appendix A5. All pyroxene are

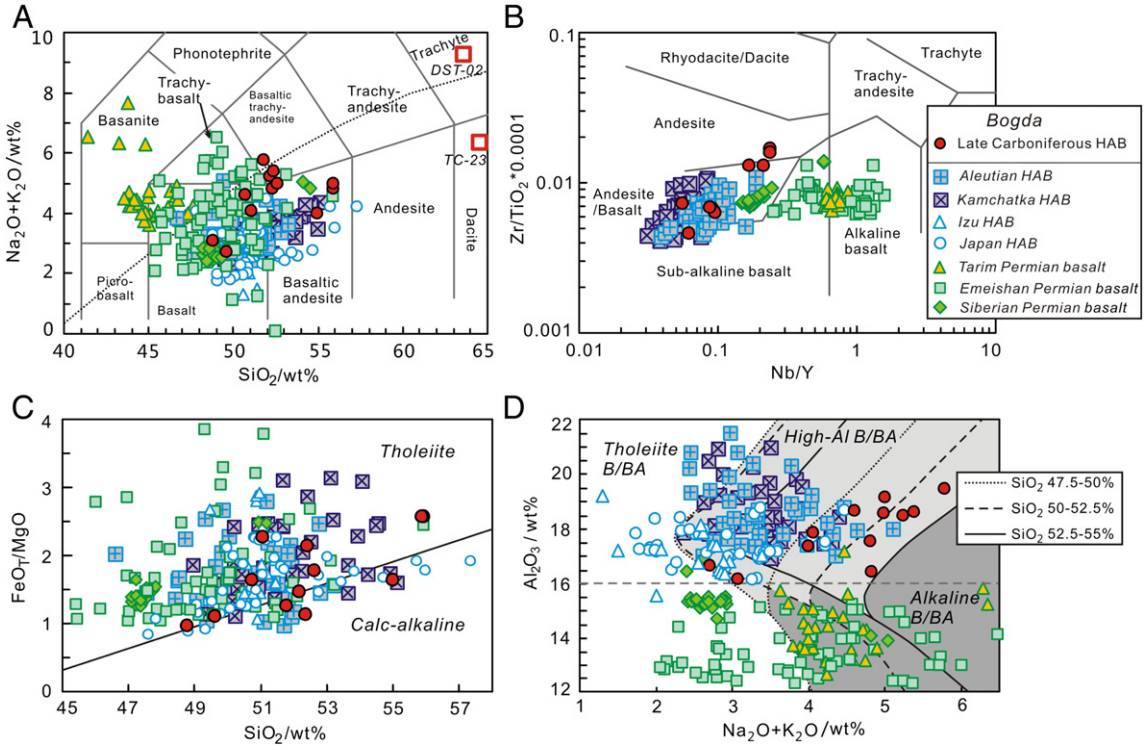

Fig. 5. Petrochemical diagrams: A) Total alkalis vs. Silica diagram (TAS, Le Maitre, 1989) Two felsic ignimbrites (DST-02 and TC-23) for U–Pb dating are also plotted. B) Zr/TiO_2 versus Nb/Y (Winchester and Floyd, 1977). C) FeO_T/MgO vs. SiO_2 diagram for the sub-alkaline basaltic samples (Miyashiro, 1974). D) Al_2O_3–Na_2O + K_2O–silica diagram (Kuno, 1960). HAB, high-Al basalt and basaltic andesite. Data sources: Three Bogda Late Carboniferous samples are from Gu et al. (2000) and Liang et al. (2011). Modern arcs: Singer et al. (2007), Kimura and Ariskin (2014), and Simon et al. (2014). Large igneous provinces: Zhou et al. (2009), Wei et al. (2014), Xu et al. (2001), L. Xiao et al. (2004), Zhang et al. (2006), Hawkesworth et al. (1995).

high-CaO (18–22% CaO) augite and salite (belong to clinopyroxene) with an end-member composition of $Wo_{36-47}En_{35-45}Fs_{11-20}$ (Fig. 9A). Some of these clinopyroxenes (Cpx) show sector and oscillatory zoning. Relative to their rims, the cores of the sector-zoned Cpx all show lower Mg# and higher Al_2O_3 whereas the oscillatory-zoned Cpx has cores with higher Mg# and lower Al_2O_3 (Fig. 9D, E; Appendix A5). In terms of mineral composition, plagioclase (Pl) in the Bogda high-Al basalt can be classified as bytownite and labradorite (Appendix A6) with an end-member composition of $An_{52-74}Ab_{26-46}Or_{0.4-2.4}$ (Fig. 9B).

6. Discussion

Effect of alteration on the geochemistry of the Bogda HABs cannot be ignored given their relatively high LOI (2.3–5.2%). The lack of correlation

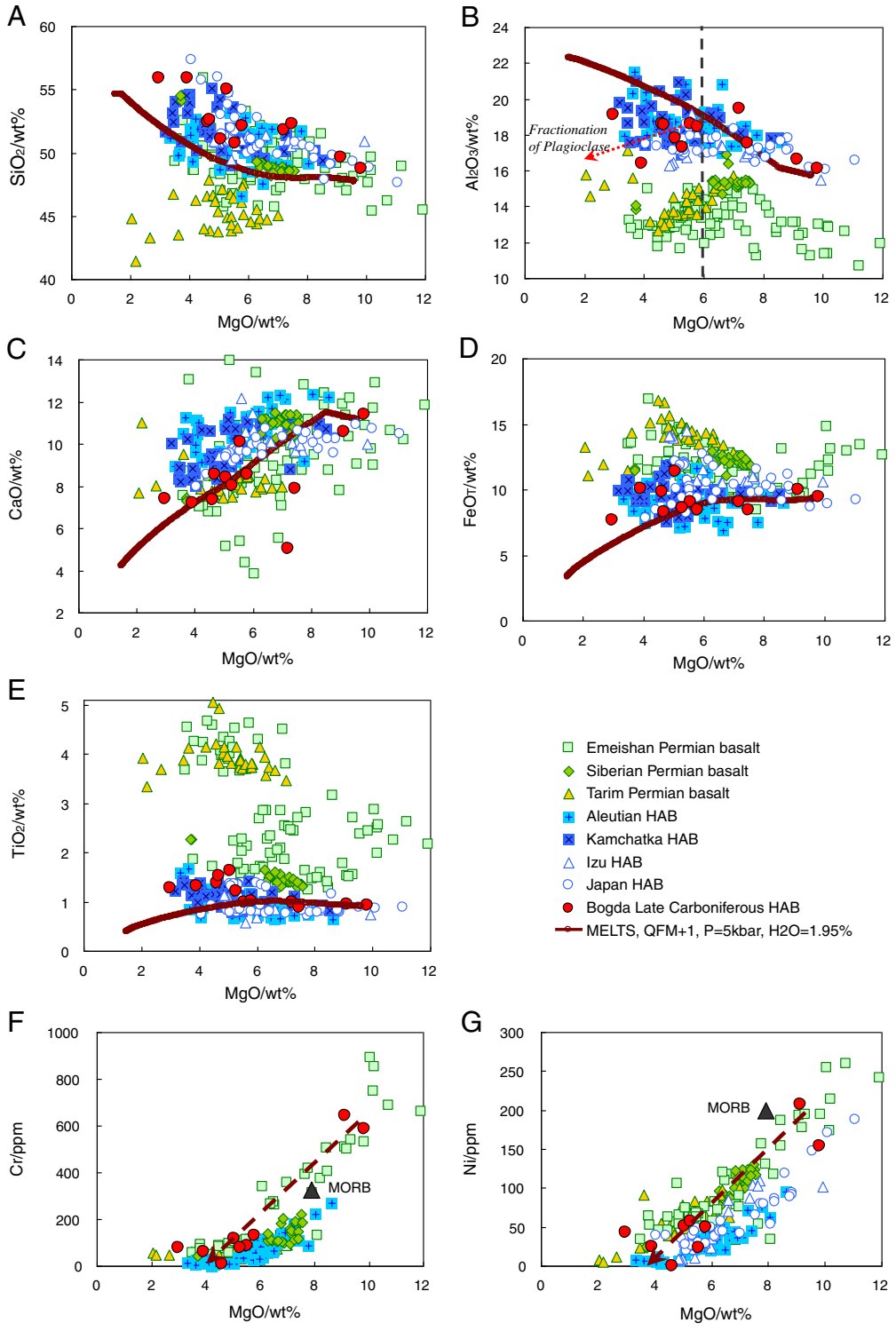

Fig. 6. Binary diagrams of oxides, Cr and Ni versus MgO. In Figs. F, G, MORB (*Black triangle*) is cited from Arevalo and McDonough (2010). Data sources are the same as in Fig. 5. The crimson curve is the liquid curve by MELTS crystallization modeling, showing the Bogda HABs are mainly controlled by high crystallization pressure.

between Rb, Ba, K, Sr, and Zr (Fig. 10) indicates that these large ion lithosphile elements were mobile during post-magmatic alteration (Polat and Hofmann, 2003). In contrast, REE, Nb, Hf, Th, U, and Pb show positive correlations with Zr, suggesting that these elements remain essentially immobile during surface processes. Hence, in the following discussion, we mainly focus on the abundances and ratios of immobile elements. The studied samples have rather uniform Nd–Hf–Pb isotopes, suggesting that their isotopic values are not significantly affected during post-magmatic alteration and can be used to discuss magmatic processes.

6.1. Rapid dynamic crystallization for the Bogda HABs

In the Bogda case, both high-MgO and low-MgO HABs are present and show essentially same trace element composition and Nd–Hf–Pb isotopes. This suggests that the two rock types share a similar petrogenesis and their compositional difference can be related each other through fractional crystallization. The Bogda HABs exhibit coherent trends between the oxides (Fig. 6), suggesting that they underwent various degrees of fractional crystallization. The Cr and Ni contents decrease from the high-MgO to the low-MgO HAB, consistent with the early crystallization of Cr-spinel and olivine. For the samples with MgO > 6 wt%, Al_2O_3 increases and CaO decreases with decreasing MgO, indicating fractional crystallization of clinopyroxene rather than plagioclase. The turning points occur for the samples with less than 6 wt%, pointing to that the fractionation of plagioclase (Fig. 6B). FeO_T and TiO_2 show limited increase as MgO decreases, arguing against significant crystallization of magnetite in the Bogda HABs.

The development of sector and oscillatory zoning in clinopyroxene is commonly attributed to disequilibrium and kinetic effects as rapid dynamic crystallization during magma ascent (Brophy et al., 1999; Downes, 1974; Lofgren et al., 2006; Schwandt and McKay, 2006). Crystallization pressure and temperature of such rapid dynamic crystallization may decrease as magma ascent from the depth to the surface and relevant information is registered in Cpx phenocrysts. The clinopyroxene–liquid thermobarometers proposed by Putirka et al. (2003) is applied as they are appropriate for both the dry and wet lavas. Only the samples least affected by alteration are considered for calculation. We used the whole rock compositions after deducing compositions of phenocrysts to represent the liquid content (see the Appendix A4). The clinopyroxenes with $KD_{Fe-Mg}^{Cpx-liquid}$ (0.2–0.4; Putirka, 2008) is assumed to be in equilibrium with the liquid. The calculated and observed values for the Cpx components are also very similar (Fig. 9C). Such a practice yields the crystallization temperature of 1203–1136 °C and pressure of 4.8–0.8 kbar for the Bogda low-MgO HABs (Appendix A5; Fig. 9). This suggests that the Bogda HABs were not formed in a relatively steady magma chamber. As shown in Fig. 9, the calculated temperatures for the sector and oscillatory-zoned Cpx have restricted variation (1164–1136 °C) while the pressures show a large variation (oscillatory-zoned Cpx 4.4–1.4 kbar; sector-zoned Cpx 2.1–0.8 kbar). These results are thus consistent with the idea that the sector and oscillatory zoning in clinopyroxene is largely related to rapid dynamic crystallization during magma ascent (Fig. 13; Brophy

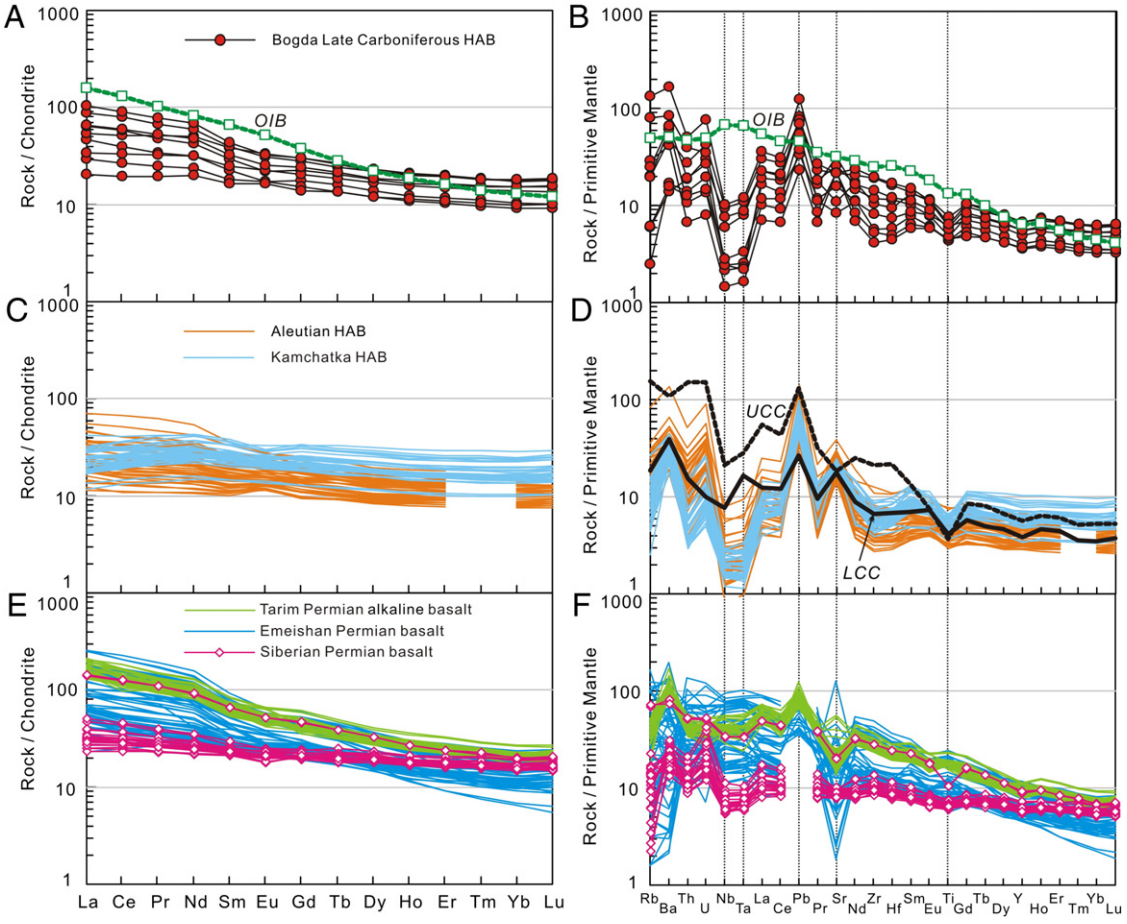

Fig. 7. Chondrite-normalized REE diagrams (A, C, E) and primitive mantle-normalized multi-element variation diagrams (B, D, F). Normalizing values and OIB are from Sun and McDonough (1989). The values of upper continental crust (UCC) and lower continental crust (LCC) are from Rudnick and Gao (2003). Data sources: Modern arcs: Singer et al. (2007) and Simon et al. (2014). Large igneous provinces: Zhou et al. (2009), Wei et al. (2014), L. Xiao et al. (2004), Zhang et al. (2006), Hawkesworth et al. (1995).

et al., 1999; Downes, 1974; Lofgren et al., 2006; Schwandt and McKay, 2006).

6.2. Subduction-modified, depleted mantle source for the Bogda HABs

The Bogda HABs are characterized by strong depletion in Nb and Ta (Fig. 7B). These geochemical signatures can be related to crustal contamination or magma mixing during the ascent of magmas or reflect that of magma source. Nevertheless, crustal contamination or magma mixing en route can be ignored given the following considerations: (1) the Bogda HABs have high and homogeneous $\varepsilon_{Nd(t)}$ (6.75–7.43) and $\varepsilon_{Hf(t)}$ (12.7–14.7), despite their relatively large variation of SiO_2 (48.8–56%). These data imply that they were essentially unaffected by crust-level processes (<1% crustal contamination or magma mixing, Fig. 8). (2) $\varepsilon_{Nd(t)}$ and $(^{206}Pb/^{204}Pb)_t$ show limited variation against Sm/Nd and SiO_2 (Fig. 11C, D), arguing against crustal contamination or magma mixing (Vervoort et al., 1999). Thus, the MORB-like Nd–Hf–Pb isotopes and arc-like trace element features of the Bogda HABs are inherited from their source.

In subduction zones, the magmatism is characterized by depletion in high field strength elements as refractory minerals such as rutiles in the arc magma source that have retained the HFSE, but is enriched in LILE (such as Rb, Sr, Ba, Pb) and Th and U due to the addition of subducted input (e.g., Hawkesworth et al., 1997; Keppler, 1996; Pearce and Peate, 1995). Likewise, the negative Nb–Ta and Ti anomalies of the volcanics along arc zones and active continental margins have been argued to result from retained rutile during melting of subducted input (e.g., Ayers and Watson, 1993; Elliott et al., 1997; Stolz et al., 1996). Thus, the strong negative Nb–Ta and minor negative Ti anomalies of the Bogda HABs are most likely due to rutile retention in the magma source (Fig. 12A). As shown in Fig. 12, the Bogda HABs have the relatively large variation of Th/Nb (0.3–0.93) with the low and restricted U/Th (0.22–0.4) and Pb/Ce (0.1–0.2), pointing to the effect of sediment-derived component (Elliott et al., 1997; Hawkesworth et al., 1997; Miller et al., 1994; Singer et al., 2007).

Chauvel et al. (2008, 2009) outlined the MORB + OIB and Island Arc arrays on the $\varepsilon_{Hf(t)}$ versus $\varepsilon_{Nd(t)}$ diagram (Fig. 8A). They discussed further that the "Island Arc array" could be generated by the mixing of depleted mantle and subducted sediments (Chauvel et al., 2009). In Fig. 8A, the Bogda HABs plot between the MORB + OIB and Island Arc arrays, suggesting a mixing between depleted mantle and subducted sediments. The depleted, MORB-like Nd–Hf isotopes suggest less than around 1% sedimentary input for the mantle source of the Bogda HABs. Such an amount (<1%) of sedimentary input would have a minor effect on their Nd–Hf–Pb isotopes, but it controls the budget of the large ion lithophile elements (such as U, Th, Pb; Fig. 12). We thus propose that the Bogda HABs were generated from a mantle wedge, which was metasomatized by sediment-derived melt (<1%).

6.3. Factors controlling high Al contents in the Bogda HABs

Previous studies suggest that the key factor for the genesis of high alumina is the delayed plagioclase nucleation (Ariskin, 1999; Brophy, 1989; Crawford et al., 1987; Eason and Sinton, 2006; Green et al., 1967; Ozerov, 2000; Sisson and Grove, 1993a, 1993b), and/or preferential accumulation or flotation of plagioclase (Crawford et al., 1987; Yoder and Tilley, 1962). Crawford et al. (1987) proposed that liquids with low-MgO (<7 wt%) and high-Al (Al_2O_3 > 18 wt%) contents never exist in nature and such a peculiar composition may be related to accumulation of plagioclase phenocrysts. However, Beard and Lofgren (1992) argued that plagioclase accumulation is not necessarily required to explain the petrogenesis of HAB. According to MELTS modeling (Asimow and Ghiorso, 1998; Ghiorso and Sack, 1995), Al_2O_3 content in liquid could reach >18 wt% through fractional crystallization under hydrous and/or high pressure conditions. This, together with the weak negative to positive Eu anomaly and the relationship between Al_2O_3 and MgO of the Bogda samples (Figs. 6B, 7A), argues against the role of accumulation or flotation of plagioclase in the genesis of the Bogda HABs.

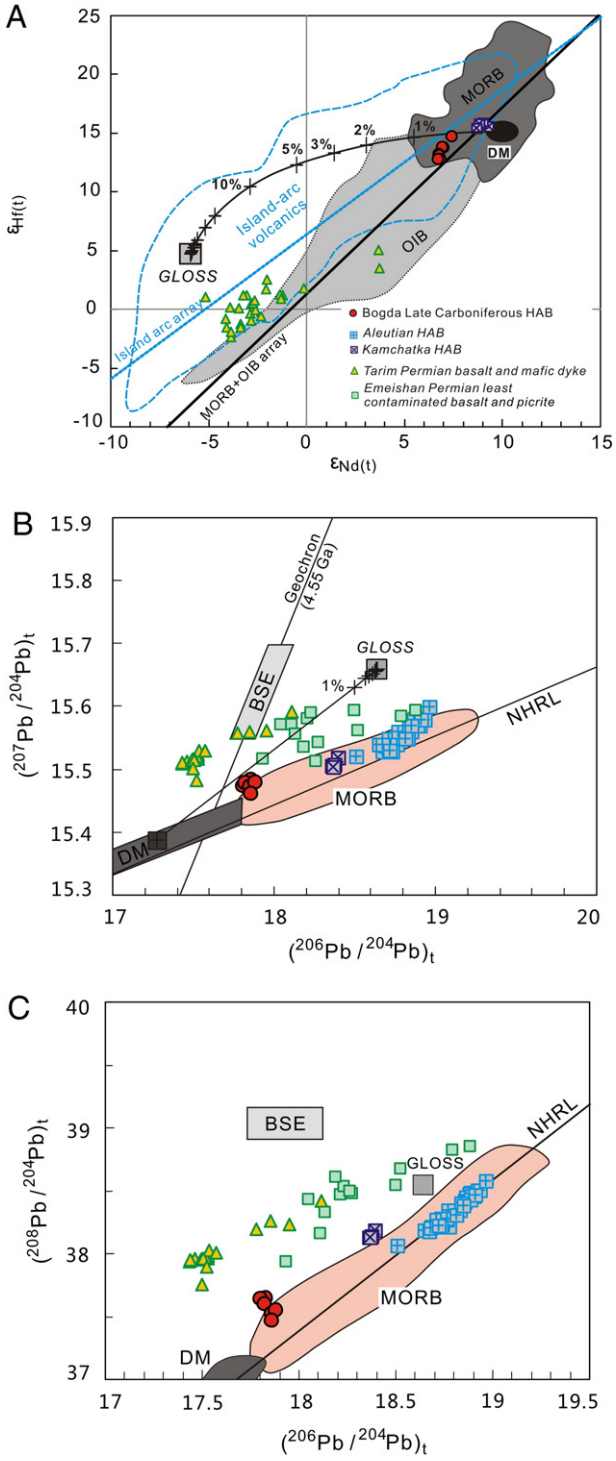

Fig. 8. Plots of initial Nd, Hf, and Pb isotopic compositions. In Nd–Hf isotope plot, the MORB + OIB and Island Arc arrays and fields for MORB, OIB, and Island-arc volcanics are from Chauvel et al. (2008, 2009). The $\varepsilon_{Nd(t)}$ and $\varepsilon_{Hf(t)}$ values of depleted mantle (DM) are assumed as +10 and +15, respectively. The Northern Hemisphere Reference Line (NHRL, Hart, 1984) is shown. Approximate locations of mantle end-members (Zindler and Hart, 1986) are indicated for reference. Data sources: DM and GLOSS are from Chauvel et al. (2009), Plank and Langmuir (1998), Salters and Stracke (2004), and Workman and Hart (2005). All of the end-members are normalized to ~315 Ma. Modern arcs: Singer et al. (2007) and Simon et al. (2014). Large igneous provinces: Li et al. (2012), Wei et al. (2014), Zhang et al. (2006).

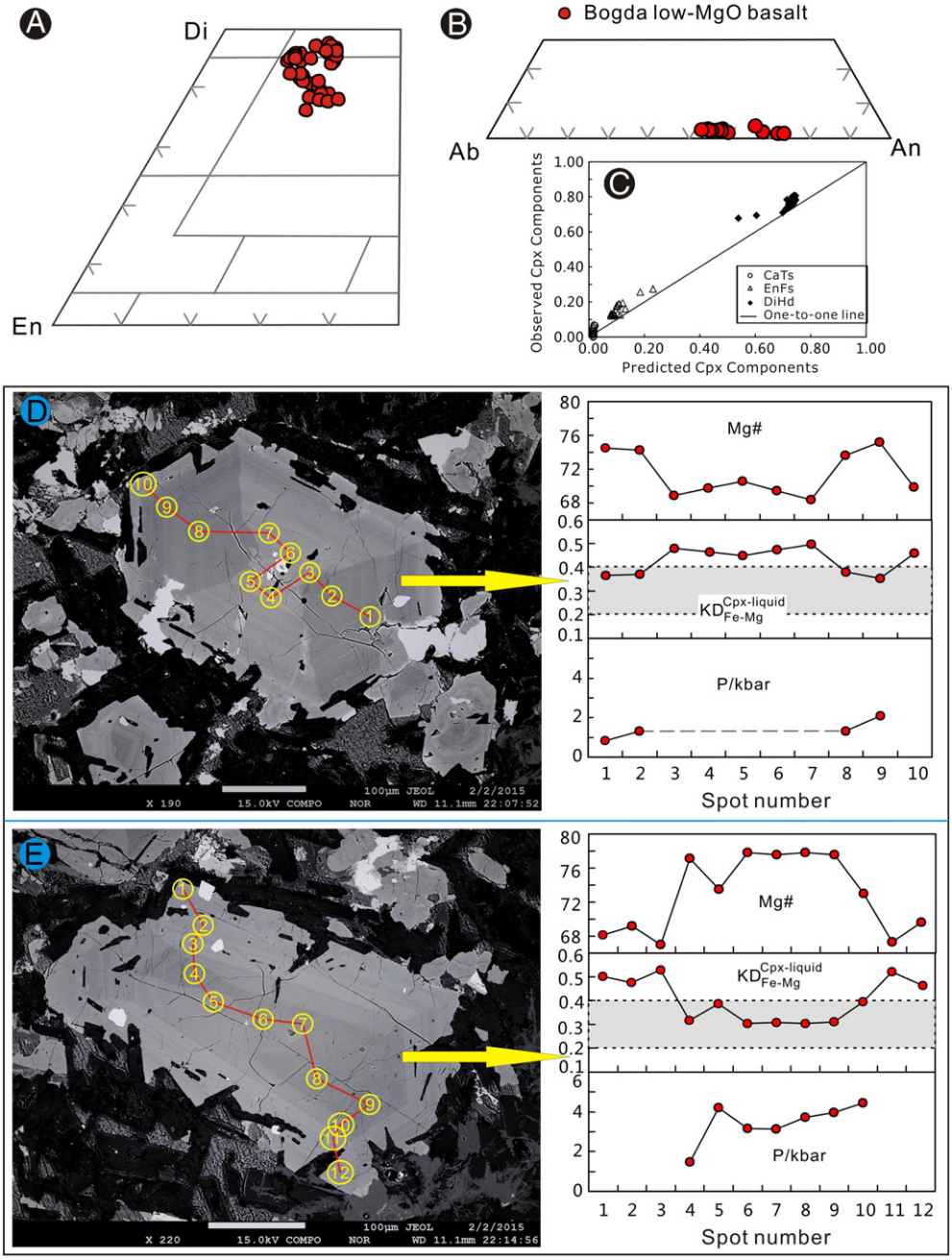

Fig. 9. (A, B) Diagrams of normative En–Fs–Wo for clinopyroxene (Cpx) and An–Ab–Or for plagioclase (Pl). Pyroxene discrimination lines are from Polderraart and Hess (1951). Di, diopside; En, enstatite; Ab, albite; An, anorthite. (C) The observed vs. predicated values for the Cpx components calculated by the clinopyroxene–liquid thermobarometers proposed by Putirka et al. (2003). (D, E) Back-scattered electron images of sector zoning and oscillatory zoning of clinopyroxene phenocrysts from the Bogda low-MgO basalt. Analysis spot numbers are shown in the images. The variation of Mg#, $KD_{Fe-Mg}^{Cpx-liquid}$, and pressure are also shown alongside.

Through wet melting experiments and direct measurements of H_2O in melt inclusions, many workers believe that water ($H_2O > 2\%$) plays a dominate role in the formation of calc-alkaline HAB (Ariskin, 1999; Beard and Lofgren, 1992; Grove et al., 2012; Kelley et al., 2010; Sisson and Grove, 1993a, 1993b). Nevertheless, others proposed that a tholeiite HAB is close to an anhydrous composition in which high pressure suppresses plagioclase fractionation (Bartels et al., 1991; Crawford et al., 1987; Draper and Johnston, 1992; Eason and Sinton, 2006; Grove et al., 1982; Le Voyer et al., 2010; Sisson and Bronto, 1998). Based on studying on the Aleutian magmas, Zimmer et al. (2010) proposed to use the Tholeiitic Index (THI) to calculate the magmatic water. Their formula is used to calculate THI of the Bogda HABs, which is 1.05. Corresponding pre-eruptive magmatic H_2O is 1.93 wt%. Water content in arc basaltic magma can be also estimated by plagioclase–liquid hygrometer (e.g., Ushioda et al., 2014). Assuming that whole rock composition after deducting compositions of phenocrysts to represent the liquid content (Appendix A4), the application of this hygrometer on sample TC-14 with the highest An (73.7) yields 1.95% as the maximum pre-eruptive magmatic H_2O of the Bogda HABs. This estimate is in good agreement with that obtained by the empirical method of Zimmer et al. (2010), testifying the robustness of calculation. The plausible low water content ($H_2O < 2\%$) is in agreement with lack of hydrous phases in the Bogda HABs, and further highlights the major role of pressure in the generation of the Bogda HABs.

Numerous studies have suggested that the high-MgO anhydrous or slightly hydrous tholeiite HAB can be generated by some extents of

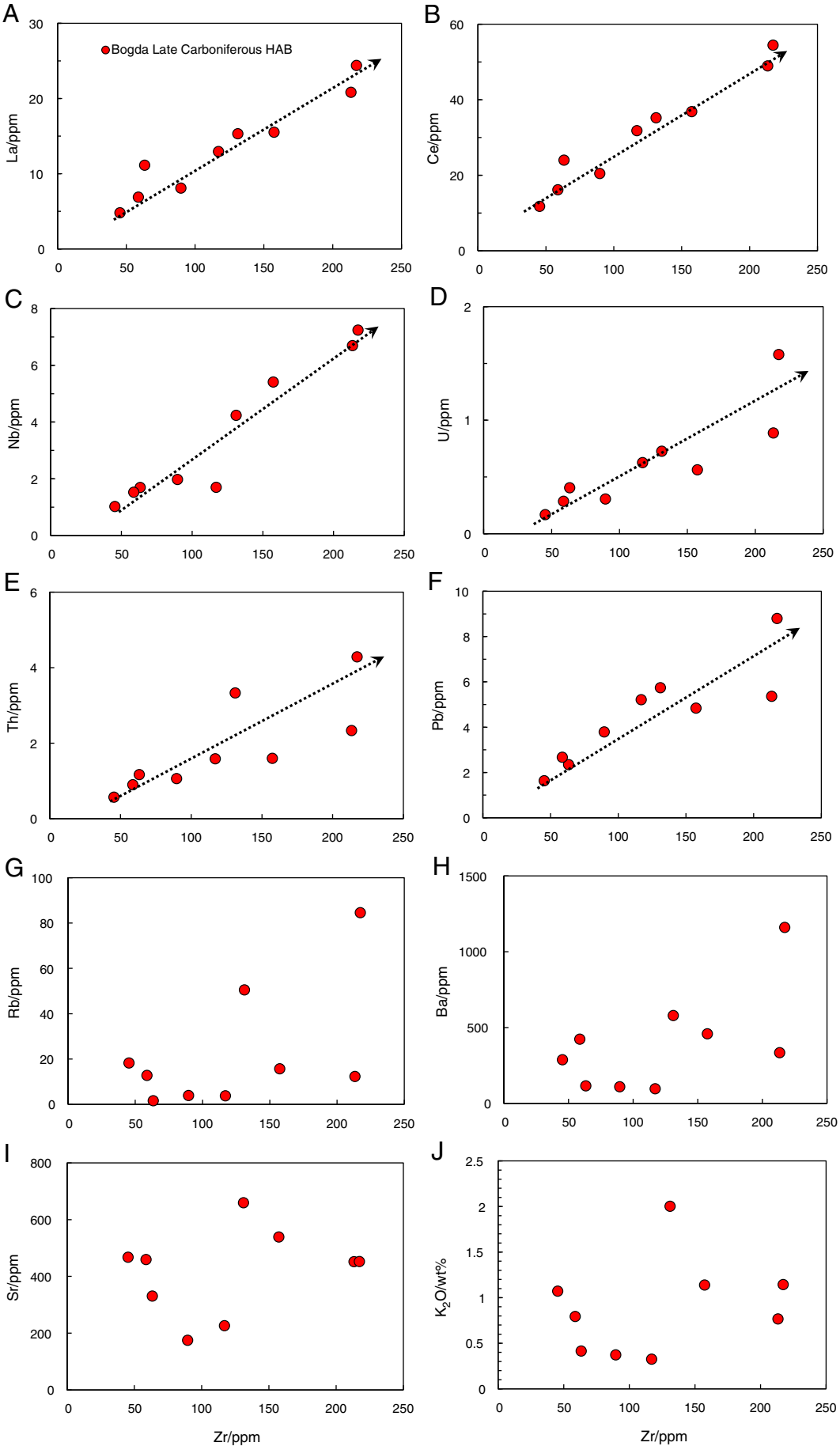

Fig. 10. Bivariate trace element plots to determine the extent of correlation of various immobile and mobile trace elements.

crystal fractionation from primary magma with higher Mg# at high pressure (5–10 kbar) near the arc crust–mantle boundary (Bartels et al., 1991; Falloon and Green, 1987; Fujii and Scarfe, 1985; Green et al., 1967; Gust and Perfit, 1987). This contrasts with the low crystallization pressure (1–2 kbar) and high water content (2–4 wt%) proposed for low-MgO calc-alkaline HAB (Sisson and Grove, 1993a). The estimated crystallization pressure of the Bogda low-MgO HAB with low H_2O (<2%) is from 4.8 to 0.8 kbar. Similar or higher crystallization pressures than 4.8 kbar can thus be reasonably inferred for the Bogda high-MgO HAB, which account for the high Al contents in these lavas (Fig. 13). Calculation by MELTS program (Asimow and Ghiorso, 1998; Ghiorso and Sack, 1995) further lends supports to the idea that high Al content is due to delayed plagioclase nucleation by high crystallization pressure (Fig. 6).

6.4. Implication for regional tectonic evolution

Two different main models have been proposed for the evolution of the B–H belt: 1) a Carboniferous island arc that was subsequently superimposed by a Permian post-collisional orogenic belt (Chen et al., 2011; Laurent-Charvet et al., 2003; Ma et al., 1997; Shu et al., 2011; W.-J. Xiao et al., 2004; Yuan et al., 2010); 2) a Carboniferous–Permian continental rift associated with a mantle plume (Gu et al., 2000, 2001; Xia et al., 2008, 2012). The second model is built on the basis of Carboniferous bimodal volcanism (Gu et al., 2000, 2001). However, the occurrence of bimodal volcanism just implies an extensional environment rather than being exclusively associated with a continental rift. A rift model is also favored by Xia et al. (2008, 2012) given the angular unconformity between the Carboniferous and the pre-Carboniferous strata. They attributed the arc-like trace compositions to crustal contamination. As discussed above, we, however, suggest that the concerned samples were essentially unaffected by crust-level processes.

To further assess the nature of Late Carboniferous volcanics, we compare them with those of Permian large igneous provinces, notably the Siberia traps (Hawkesworth et al., 1995), Emeishan traps (Qi and Zhou, 2008; L. Xiao et al., 2004; Xu et al., 2001; Zhang et al., 2006), and Tarim basalts (Li et al., 2012; Wei et al., 2014; Zhou et al., 2009). The latter are widely interpreted to be the melting products of mantle plumes. The comparison suggests that the Bogda Late Carboniferous HABs are different from the mantle plume-related basalts in many aspects:

1) In general, the Bogda HABs have higher Al_2O_3 (16.1–21.1%), SiO_2 (48.8–56%), and lower FeO_T (7.65–11.4%), TiO_2 (0.94–1.82%) than mantle plume-related basalts (Figs. 5, 6).
2) In Fig. 11A, B, the Bogda HABs plot in the field of arc basalts, whereas, except for some Siberian samples, the Tarim and Emeishan basalts plot in the field of continental flood basalts. Furthermore, the Bogda HAB have lower Nb/La (<0.5, except one sample) and higher Pb/Ce (>0.1) than those mantle plume-related basalts (Nb/La = 0.6–1.7, Pb/Ce = 0.04–0.1; Fig. 12). Low-Ti lavas from the Siberian and Emeishan Traps also show depletion in Nb–Ta. However, these low-Ti basalts have higher Nb/La and lower Pb/Ce ratios than the Bogda HABs and are interpreted to be derived from the enriched

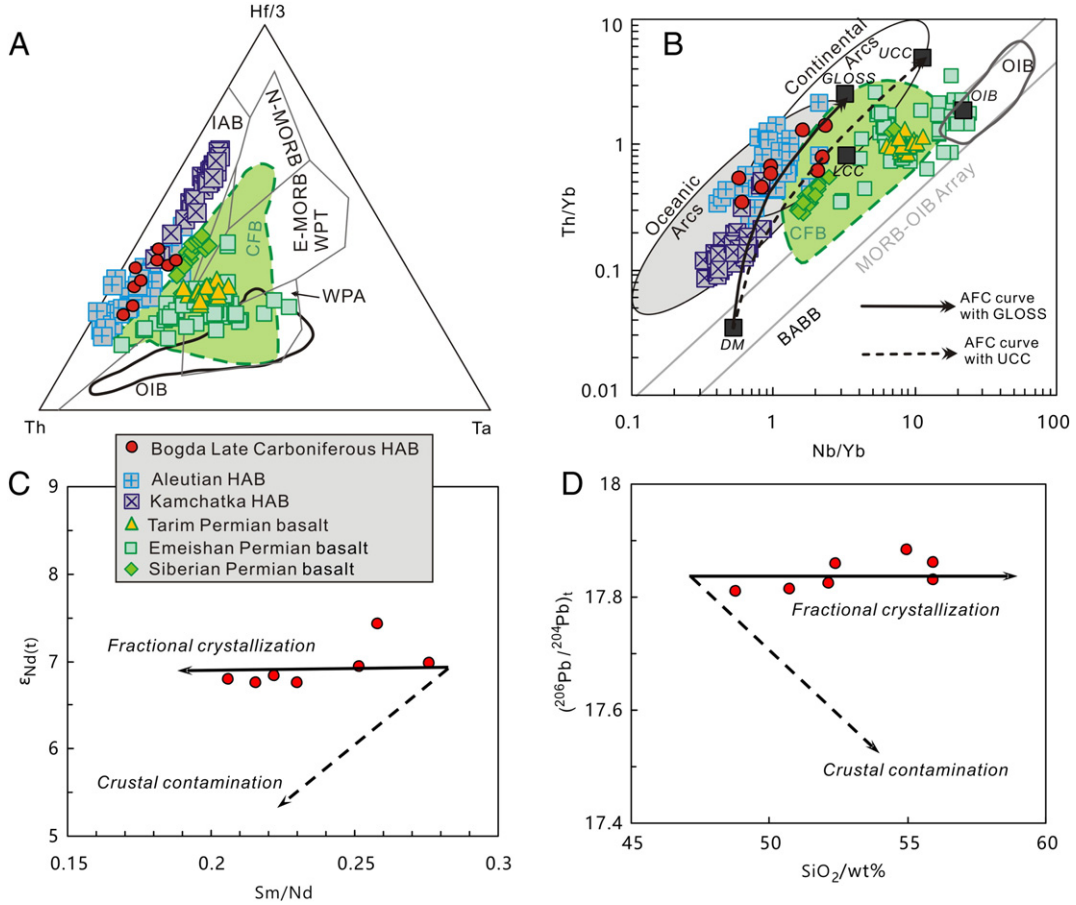

Fig. 11. (A) Th–Hf–Nb discrimination diagram (Wood, 1980). (B) Th/Yb versus Nb/Yb diagram (modified from Pearce, 2014). AFC with GLOSS/UCC = assimilation fractional crystallization of DM with GLOSS or UCC. (C, D) Plots of $\varepsilon_{Nd(t)}$ versus Sm/Nd and $(^{206}Pb/^{204}Pb)_t$ versus SiO_2 to assess the effect of crustal contamination on the compositions of the Bogda Late Carboniferous HAB. In Figs. A and B, the latest fields of CFB (continental flood basalts), OIB are cited from C. Li et al. (2015). Data sources: DM (depleted mantle), OIB and GLOSS are cited from Salters and Stracke (2004), Sun and McDonough (1989), and Plank and Langmuir (1998), respectively. UCC (upper continental crust) and LCC (lower continental crust) are from Rudnick and Gao (2003). Modern arcs: Singer et al. (2007) and Simon et al. (2014). Large igneous provinces: Zhou et al. (2009), Wei et al. (2014), L. Xiao et al. (2004), Zhang et al. (2006), and Hawkesworth et al. (1995).

continental lithospheric mantle (Hawkesworth et al., 1995; L. Xiao et al., 2004).

3) The Bogda HABs have higher $\varepsilon_{Nd(t)}$ (5.87–8.25) than those mantle plume-related basalts ($\varepsilon_{Nd(t)} < 5$; Figs. 8, 12). They also have higher $\varepsilon_{Hf(t)}$ and lower $(^{207}Pb/^{204}Pb)_t$ and $(^{208}Pb/^{204}Pb)_t$ ratios than the mantle plume-related basalts (Fig. 8).

In addition, the volume of the basaltic lavas in the Chinese North Tianshan is much smaller than those of the Siberian, Emeishan, and Tarim basalts (e.g., Hawkesworth et al., 1995; Wei et al., 2014; Xu et al., 2001). All these indicate that the "plume hypothesis" cannot adequately be applied to the Carboniferous magmatism in the Tianshan orogenic belt (Zhu et al., 2009).

HAB commonly occurs in arc settings, with modern examples at Aleutian, NE Japan, South Sandwich, Izu–Bonin–Mariana, Vanuatu, Tonga–Kermadec, and Kurile–Kamchatka island arcs (Crawford et al., 1987; Kuno, 1960; Ozerov, 2000; Sisson and Grove, 1993a and references therein), or mid-ocean ridges, such as the Galápagos Spreading Center (Eason and Sinton, 2006). Our new zircon SHRIMP U–Pb ages for the felsic ignimbrites (319 ± 3 Ma and 315 ± 2 Ma) suggest that the Bogda HABs were formed in the Late Carboniferous. Therefore, the B–H belt was most likely an island arc system during the Late Carboniferous (W.-J. Xiao et al., 2004), rather than an intraplate setting. Other supporting evidence for a Carboniferous arc setting include (a) in the B–H belt, it lacks Cambrian and Precambrian strata. The oldest sedimentary strata are the Ordovician to Silurian marine strata (Huangcaopo Group; Ma, 1999). (b) Devonian to Carboniferous arc tholeiite and calc-alkaline basalt–andesites are widespread in the region (Ma et al., 1997). The Kelameili and Bayinggou ophiolites nearby the B–H belt are the youngest ophiolites (325–345 Ma) in Xinjiang province, NW China (Jian et al., 2005; Wang et al., 2009; Xu et al., 2006a, 2006b). They probably represent remnants of the Paleo-Tianshan Ocean (Han et al., 2010; W.-J. Xiao et al., 2004; Xiao et al., 2008). Thus, the B–H belt could be a Devonian to Carboniferous island arc system related with

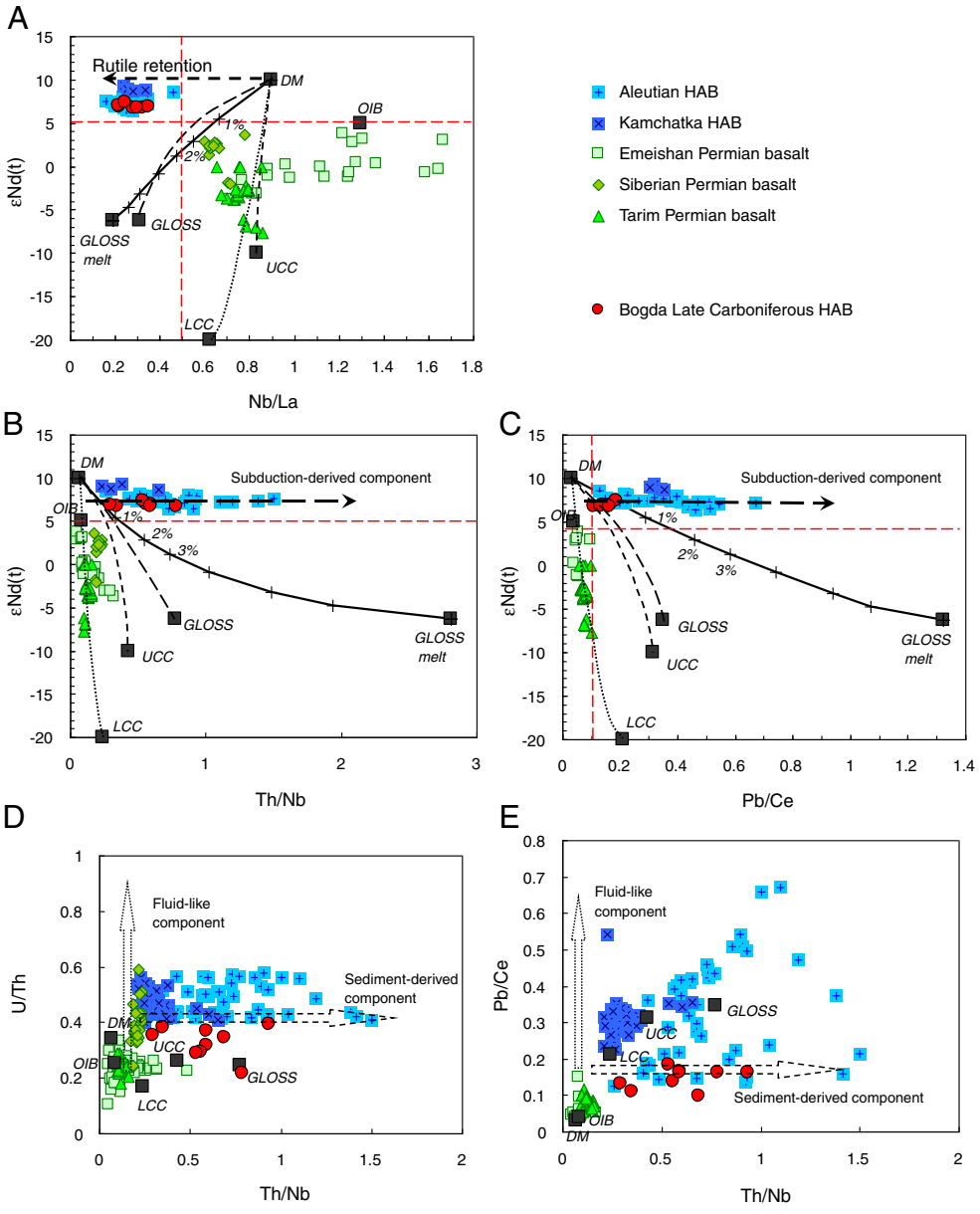

Fig. 12. Plots of $\varepsilon_{Nd(t)}$ versus Nb/La (A), Th/Nb (B), Pb/Ce (C) and U/Th (D), Pb/Ce (E) versus Th/Nb. The $\varepsilon_{Nd(t)}$ values of N-MORB, OIB, UCC and LCC are assumed as +10, +5, −10 and −20, respectively. In Figs. A to C, the solid and dashed curves represent AFC ($r = 0.5$; DePaolo, 1981; Powell, 1984) of DM with GLOSS melt, GLOSS, UCC, or LCC. The crystallized contents of every mineral are approximately following the MELTS and the partition coefficients for calculation are listed in Appendix A7. Calculated GLOSS melt composition is assuming 5% melt of GLOSS, where sediment/melt partition coefficients are from Singer et al. (2007). Data sources are the same as in Fig. 11.

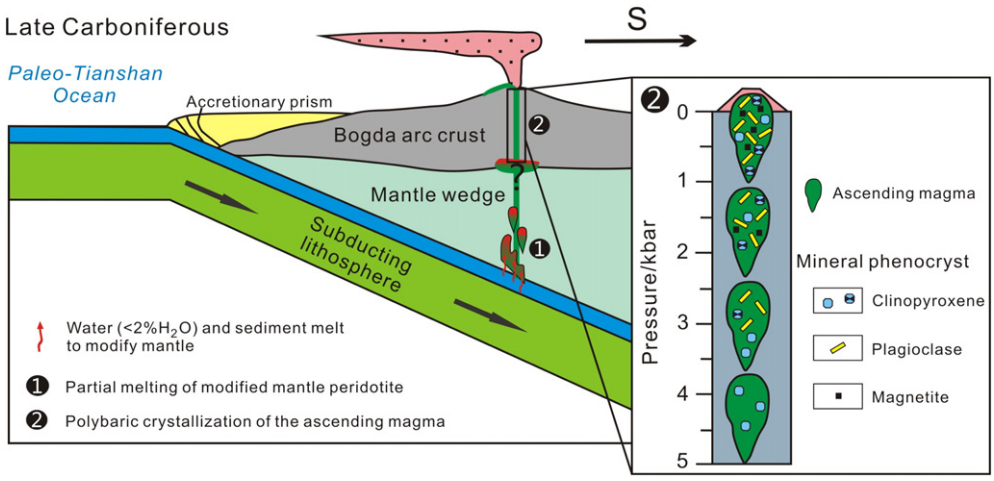

Fig. 13. Idealized schematic model for the generation of the Bogda HABs beneath the Bogda island arc system in Late Carboniferous period.

S-dipping subduction of the Paleo-Tianshan Ocean (Fig. 13; Laurent-Charvet et al., 2003; Ma et al., 1997; W.-J. Xiao et al., 2004; Yuan et al., 2010).

However, Han et al. (2010) restricted the closure of Paleo-Tianshan Ocean at the end of Early Carboniferous and suggested a subsequent post-collisional orogenic setting. Their argument was built on a ca. 316 Ma "stitching pluton" which displays some characteristics of post-collisional A-type granites (Chen et al., 2011; Han et al., 2010; Zhang and Zou, 2013). However, this "stitching pluton" shows a wide SiO_2 range (58–74%) with a metaluminous I-type affinity (Si et al., 2014). In addition, they have restricted zircon saturation temperature (T_{Zr} = 792–842 °C) in the overlapping region of the typical A-type granite and I-type granite (King et al., 1997; Liu et al., 2013; Zhong and Xu, 2009). In fact, most of Late Carboniferous felsic rocks in the Chinese Tianshan Orogenic Belts belong to I-type granitoids (Liu et al., 2013; Tang et al., 2010, 2014; Tong et al., 2010; Yan et al., 2013; Zhang et al., 2015; Zhu et al., 2009). In contrast, A-type granitoids mainly occurred in the Early Permian (N.-B. Li et al., 2015; Tang et al., 2010; Yuan et al., 2010; Zhang and Zou, 2013). We therefore favor for an arc setting for the Late Carboniferous in the Tianshan belt, consistent with recent findings of subduction-related assemblages in the western Jungar area (Tang et al., 2012). Moreover, if Han et al. (2010) were correct, the HABs identified in this study may have occurred in a post-collision or an intraplate setting. However, so far no HABs have been observed in these settings.

Nevertheless, abundant A-type granites occurred toward the end of the Carboniferous and the Early Permian. Therefore, the tectonic transition from a subduction to an intraplate setting is inferred to have taken place during the Late Carboniferous and the Early Permian, although the exact timing is difficult to determine. Such a transition was most likely a gradual rather than abrupt process and may be transient in different places in the Tianshan Orogenic belt. At some stages, subduction and locally extended setting (arc retreating) occur together and gradually evolve to an intraplate setting. This explains the co-existence of HABs and A-type granites in this area.

7. Conclusions

The HABs from the Upper Carboniferous Liushugou Formation in the Bogda Mountains (315–319 Ma) have been investigated to constrain the Carboniferous tectonic evolution in the CAOB. The MORB-like Nd–Hf–Pb isotopes and arc-like trace element compositions indicate that the Bogda HABs may have been generated from a mantle wedge, metasomatized by sediment-derived melts. Dominant fractioning phases are olivine and high-CaO (18–22% CaO) clinopyroxene, while plagioclase nucleation was likely delayed by the high crystallization pressure. The sector and oscillatory zoning in clinopyroxene phenocrysts is attributable to rapid dynamic crystallization during magma ascent. The occurrence of the Bogda HABs suggests an island arc environment, probably related to S-dipping subduction of the Paleo-Tianshan Ocean during the Late Carboniferous. This contrasts with the previously proposed model involving intraplate large igneous provinces.

Supplementary data to this article can be found online at http://dx.doi.org/10.1016/j.lithos.2016.04.005.

Acknowledgments

This study was funded by National Basic Research Program of China (2011CB808906) and GIG-CAS 135 project (Y234051001) to Yi-Gang Xu, NSFC (41503017) to Wei Xie, China Postdoctoral Science Foundation Grant (2013M542214) to Wei Xie, NSFC (415030057) to Liang Ma, and NSFC (41203009) to Zhen-Yu Luo. We thank Hang-Qiang Xie, Yin Liu, Guang-Qian Hu, Jin-Long Ma for technical help with diverse analyses. The GIGCAS publication is No. IS-2223.

References

Allen, M.B., Windley, B.F., Zhang, C., 1993. Palaeozoic collisional tectonics and magmatism of the Chinese Tien Shan, Central Asia. Tectonophysics 220, 89–115.
Arevalo, Jr.R., McDonough, W.F., 2010. Chemical variations and regional diversity observed in MORB. Chemical Geology 271, 70–85.
Ariskin, A.A., 1999. Phase equilibria modeling in igneous petrology: use of COMAGMAT model for simulating fractionation of ferro-basaltic magmas and the genesis of high-alumina basalt. Journal of Volcanology and Geothermal Research 90, 115–162.
Asimow, P.D., Ghiorso, M.S., 1998. Algorithmic modifications extending MELTS to calculate subsolidus phase relations. American Mineralogist 83, 1127–1132.
Ayers, J.C., Watson, E.B., 1993. Rutile solubility and mobility in supercritical aqueous fluids. Contributions to Mineralogy and Petrology 114, 321–330.
Bartels, K.S., Kinzler, R.J., Grove, T.L., 1991. High pressure phase relations of primitive high-alumina basalt from Medicine Lake volcano, Northern California. Contributions to Mineralogy and Petrology 108, 253–270.
Beard, J.S., Lofgren, G.E., 1992. An experiment-based model for the petrogenesis of high-alumina basalts. Science 258, 112–115.
BGMRXUAR (Bureau of Geology and Mineral Resources of Xinjiang Uygur Autonomous Region), 1993. Regional Geology of Xinjiang Autonomous Region, Geological Memoirs, no. 32, Map Scale 1:500000. Geological Publishing House, Beijing (in Chinese).
Black, L.P., Kamo, S.L., Allen, C.M., Aleinikoff, J.N., Davis, D.S., Korsch, R.J., Foudoulis, C., 2003. TEMORA 1: a new zircon standard for Phanerozoic U–Pb geochronology. Chemical Geology 200, 155–170.
Brophy, J.G., 1989. Can high-alumina arc basalt be derived from low-alumina arc basalt? Evidence from Kanaga Island, Aleutian Arc, Alaska. Gelogy 17, 333–336.
Brophy, J.G., Marsh, B.D., 1986. On the origin of high-alumina arc basalt and the mechanics of melt extraction. Journal of Petrology 27, 763–789.
Brophy, J.G., Whittington, C.S., Park, Y.-R., 1999. Sector-zoned augite megacrysts in Aleutian high alumina basalts: implications for the conditions of basalt crystallization and the generation of calc-alkaline series magmas. Contributions to Mineralogy and Petrology 135, 277–290.

Carroll, A.R., Liang, Y., Graham, S.A., Xiao, X., Hendrix, M.S., Chu, J., McKnigth, C.L., 1990. Junggar basin, northewstern China: trapped Late Paleozoic Ocean. Tectonophysics 181, 1–14.
Chauvel, C., Lewin, E., Carpentier, M., Arndt, N.S., Marini, J.-C., 2008. Role of recycled oceanic basalt and sediment in generating the Hf–Nd mantle array. Nature Geoscience 1, 64–67.
Chauvel, C., Marini, J.-C., Plank, T., Ludden, J.N., 2009. Hf–Nd input flux in the Izu–Mariana subduction zone and recycling of subducted material in the mantle. Geochemistry, Geophysics, Geosystems 10, Q01001. http://dx.doi.org/10.1029/2008GC002101.
Che, Z.C., Liu, L., Liu, H.F., 1996. Review on the ancient Yili rift, Xinjiang, China. Acta Petrologica Sinica 12, 478–490 (in Chinese with English abstract).
Chen, X., Shu, L., Santosh, M., 2011. Late Paleozoic post-collisional magmatism in the Eastern Tianshan Belt, Northwest China: new insights from geochemistry, geochronology and petrology of bimodal volcanic rocks. Lithos 127, 581–598.
Compston, W., Williams, I.S., Kirschvink, J.L., 1992. Zircon U–Pb ages for the Early Cambrian timescale. Journal of the Geological Society, London 149, 171–184.
Crawford, A.J., Falloon, T.J., Eggins, S., 1987. The origin of island arc high alumina basalts. Contributions to Mineralogy and Petrology 97, 417–430.
DePaolo, D.J., 1981. Trace element and isotopic effects of combined wallrock assimilation and fractional crystallization. Earth and Planetary Science Letters 53, 189–202.
Downes, M.J., 1974. Sector and oscillatory zoning in calcic augites from M. Etna, Sicily. Contributions to Mineralogy and Petrology 47, 187–196.
Draper, D.S., Johnston, A.D., 1992. Anhydrous PT phase relations of an Aleutian high-MgO basalt: an investigation of the role of olivine–liquid reaction in the generation of arc high-alumina basalts. Contributions to Mineralogy and Petrology 112, 501–519.
Eason, D., Sinton, J., 2006. Origin of high-Al N-MORB by fractional crystallization in the upper mantle beneath the Galápagos Spreading Center. Earth and Planetary Science Letters 252, 423–436.
Elliott, T., Plank, T., Zindler, A., White, W., Bourdon, B., 1997. Element transport from slab to volcanic front at the Mariana arc. Journal of Geophysical Research 102, 14991–15019.
Falloon, T.J., Green, D.H., 1987. Anhydrous partial meltings of MORB pyrolite and other peridiotite compositions at 10 kbar: implications for the origin of primitive MORB glasses. Mineralogy and Petrology 37, 181–219.
Fujii, T., Scarfe, C.M., 1985. Compositions of liquids coexisting with spinel lherzolite at 10 kbar and the genesis of MORBs. Contributions to Mineralogy and Petrology 90, 18–28.
Gao, J., Li, M., Xiao, X., Tang, Y., He, G., 1998. Paleozoic tectonic evolution of the Tianshan orogeny, Northwestern China. Tectonophysics 287, 213–231.
Ghiorso, M.S., Sack, R.O., 1995. Chemical mass transfer in magmatic processes IV. A revised and internally consistent thermodynamic model for the interpolation and extrapolation of liquid–solid equilibria in magmatic systems at elevated temperatures and pressures. Contributions to Mineralogy and Petrology 119, 197–212.
Goto, A., Tatsumi, Y., 1996. Quantitative analysis of rock samples by an X-ray fluorescence spectrometer (II). The Rigaku Journal 13, 20–39.
Green, T.H., Green, D.H., Ringwood, A.E., 1967. The origin of high-alumina basalts and their relationships to quartz tholeiites and alkali basalts. Earth and Planetary Science Letters 2, 41–51.
Grove, T.L., Gerlach, D.C., Sando, T.W., 1982. Origin of calc-alkaline series lavas at medicine Lake volcano by fractionation, assimilation and mixing. Contributions to Mineralogy and Petrology 80, 160–182.
Grove, T.L., Kinzler, R.J., Baker, M.B., Donnelly-Nolan, J.M., Lesher, C.E., 1988. Assimilation of granite by basaltic magma at burnt lava flow, Medicine Lake volcano, Northern California: decoupling of heat and mass transfer. Contributions to Mineralogy and Petrology 99, 320–343.
Grove, T.L., Till, C.B., Krawczynski, M.J., 2012. The role of H_2O in subduction zone magmatism. Annual Review of Earth and Planetary Sciences 40, 413–439.
Gu, L.X., Hu, S.X., Yu, C.S., Li, H.Y., Xiao, X.J., Yan, Z.F., 2000. Carboniferous volcanites in the Bogda orogenic belt of eastern Tianshan: their tectonic implications. Acta Petrologica Sinica 16, 305–316 (in Chinese with English abstract).
Gu, L.X., Hu, S.X., Yu, C.S., Zhao, M., Wu, C.Z., Li, H.Y., 2001. Intrusive activities during compression–extension tectonic conversion in the Bogda intracontinental orogen. Acta Petrologica Sinica 17, 187–198 (in Chinese with English abstract).
Gust, D.A., Perfit, M.R., 1987. Phase relations of a high-Mg basalt from the Aleutian island arc: implications for primary island arc basalts and high-Al basalts. Contributions to Mineralogy and Petrology 97, 7–18.
Hamada, M., Fujii, T., 2008. Experimental constraints on the effects of pressure and H_2O on the fractional crystallization of high-Mg island arc basalt. Contributions to Mineralogy and Petrology 155, 767–790.
Han, B.-F., Guo, Z.-J., Zhang, Z.-C., Zhang, L., Chen, J.-F., Song, B., 2010. Age, geochemistry, and tectonic implications of a Late Paleozoic stitching pluton in the North Tian Shan suture zone, Western China. Geological Society of America Bulletin 122, 627–640.
Hart, S.R., 1984. A large-scale isotope anomaly in the Southern Hemisphere mantle. Nature 309, 753–757.
Hawkesworth, C.J., Lightfoot, P.C., Fedorenko, V.A., Blake, S., Naldrett, A.J., Doherty, W., Gorbachev, N.S., 1995. Magma differentiation and mineralisation in the Siberian continental flood basalts. Lithos 34, 61–88.
Hawkesworth, C., Turner, S., Peate, D., McDermott, F., Calsteren, P., 1997. Elemental U and Th variations in island arc rocks: implications for U-series isotopes. Chemical Geology 139, 207–221.
He, G.Q., Li, M.S., Liu, D.Q., Tang, Y.L., Zhou, R.H., 1994. Palaeozoic Crustal Evolution and Mineralization in Xinjiang of China. Xinjiang People's Publication House, Urumqi, p. 437 (in Chinese with English abstract).
Jian, P., Liu, D.Y., Shi, Y.R., Zhang, F.Q., 2005. SHRIMP dating of SSZ ophiolites from Northern Xinjiang Province, China: implications for generation of oceanic crust in the Central Asian Orogenic Belt. In: Sklyarov, E.V. (Ed.), Structural and Tectonic Correlation across the Central Asia Orogenic Collage: North-Eastern Segment. Guidebook and Abstract Volume of the Siberian Workshop IGCP-480. IEC SB RAS, Irkutsk, pp 246.
Johnson, A.D., 1986. Anhydrous P–T phase relations of near-primary high-alumina basalt from the South Sandwich Islands. Contributions to Mineralogy and Petrology 92, 368–382.
Kelley, K.A., Plank, T., Newman, S., Stolper, E.M., Grove, T.L., Parman, S., Hauri, E.H., 2010. Mantle melting as a function of water content beneath the Mariana Arc. Journal of Petrology 51, 1711–1738.
Keppler, H., 1996. Constraints from partitioning experiments on the composition of subduction-zone fluids. Nature 380, 237–240.
Kimura, J.-I., Ariskin, A.A., 2014. Calculation of water-bearing primary basalt and estimation of source mantle conditions beneath arcs: PRIMACALC2 model for WINDOWS. Geochemistry, Geophysics, Geosystems 15, 1494–1514. http://dx.doi.org/10.1002/2014GC005329.
King, P.L., White, A.J.R., Chappell, B.W., Allen, C.M., 1997. Characterization and origin of aluminous A-type granites from the Lachlan Fold Belt, Southeastern Australia. Journal of Petrology 38, 371–391.
Kuno, H., 1960. High-alumina basalt. Journal of Petrology 1, 121–145.
Laurent-Charvet, S., Charvet, J., Monie, P., Shu, L., 2003. Late Paleozoic strike-slip shear zones in eastern central Asia (NW China): new structural and geochronological data. Tectonics 22, 1009–1032.
Le Maitre, R.W., 1989. A classification of igneous rocks and glossary terms: recommendations of the International Union of Geological Sciences Subcommission on the Systematics of Igneous Rocks. Blackwell Scientific Publications, Trowbridge, Wilts, UK, pp. 1–193.
Le Voyer, M., Rose-Koga, E.F., Shimizu, N., Grove, T.L., Schiano, P., 2010. Two contrasting H_2O-rich components in primary melt inclusions from Mount Shasta. Journal of Petrology 51, 1571–1595.
Li, X.-H., Li, Z.-X., Wingate, M.T.D., Chung, S.-L., Liu, Y., Lin, G.-C., Li, W.-X., 2006. Geochemistry of the 755 Ma Mundine well dyke swarm, Northwestern Australia: part of a Neoproterozoic mantle superplume beneath Rodinia? Precambrian Research 146, 1–15.
Li, Z.L., Li, Y.Q., Chen, H.L., Santosh, M., Yang, S.F., Xu, Y.G., Langmuir, C.H., Chen, Z.X., Yu, X., Zou, S.Y., 2012. Hf isotopic characteristics of the Tarim Permian large igneous province rocks of NW China: implication for the magmatic source and evolution. Journal of Asian Earth Sciences 49, 191–202.
Li, C., Arndt, N.T., Tang, Q., Ripley, E.M., 2015. Trace element indiscrimination diagrams. Lithos 232, 76–83.
Li, N.-B., Niu, H.-C., Shan, Q., Yang, W.-B., 2015. Two episodes of Late Paleozoic A-type magmatism in the Qunjisayi area, western Tianshan: petrogenesis and tectonic implications. Journal of Asian Earth Sciences 113, 238–253.
Liang, T., Guo, X., Gao, J., Fan, T., Qin, H., Zhou, R., Hei, H., 2011. Geochemistry and structure characteristic of Carboniferous volcanic rocks in the eastern of Bogeda Mountain. Xinjiang Geology 29, 289–295 (in Chinese with English abstract).
Liu, Y., Liu, H.C., Li, X.H., 1996. Simultaneous and precise determination of 40 trace elements in rock samples using ICP–MS. Geochimica 25, 552–558 (in Chinese with English abstract).
Liu, H.-Q., Xu, Y.-G., He, B., 2013. Implications from zircon-saturation temperatures and lithological assemblages for Early Permian thermal anomaly in Northwest China. Lithos 182–183, 125–133.
Lofgren, G.E., Huss, G.R., Wasserburg, G.J., 2006. An experimental study of trace-element partitioning between Ti-Al-clinopyroxene and melt: equilibrium and kinetic effects including sector zoning. American Mineralogist 91, 1596–1606.
Ludwig, K.R., 2001a. Squid 1.02. A user manual. Berkeley Geochronol Center Special Publication, Berkeley, pp. 1–219.
Ludwig, K.R., 2001b. Using Isoplot/EX, version 2.49. A Geochronological Toolkit for Microsoft Excel. Berkeley Geochronol Center Special Publication, Berkeley, pp. 1–55.
Ma, J.C., 1999. Study on the Huangcaopo Group in the eastern Junggar. Journal of Mineralogy and Petrology 19, 52–55 (in Chinese with English abstract).
Ma, R.S., Shu, L.S., Sun, J.Q., 1997. Tectonic Evolution and Metallization in the Eastern Tianshan Belt, China. Geological Publish House, Beijing, p. 202 (in Chinese with English abstract).
Marsh, B.D., 1979. Island arc development: some observations, experiments and speculations. The Journal of Geology 87, 687–713.
Marsh, B.D., 1982. The Aleutians. In: Thorpe, R.S. (Ed.), Andesites. Wiley, New York, pp. 99–114.
Miller, D.M., Goldstein, S.L., Langmuir, C.H., 1994. Cerium/lead and lead isotope ratios in arc magmas and the enrichment of lead in the continents. Nature 368, 514–520.
Miyashiro, A., 1974. Volcanic rock series in island arcs and active continental margins. American Journal of Science 274, 321–355.
Ozerov, A.Y., 2000. The evolution of high-alumina basalts of the Klyuchevskoy volcano, Kamchatka, Russia, based on microprobe analyses of mineral inclusions. Journal of Volcanology and Geothermal Research 95, 65–79.
Pearce, J.A., 2014. Immobile element fingerprinting of ophiolites. Elements 10, 101–108.
Pearce, J.A., Peate, D.W., 1995. Tectonic implications of the composition of volcanic arc magmas. Annual Review of Earth and Planetary Sciences 23, 251–285.
Pirajno, F., Mao, J.W., Zhang, Z.C., Zhang, Z.H., Chai, F.M., 2008. The association of mafic–ultramafic intrusions and A-type magmatism in the Tianshan and Altay orogens, NW China: implications for geodynamic evolution and potential for the discovery of new ore deposits. Journal of Asian Earth Sciences 32, 165–183.
Plank, T., Langmuir, C.H., 1998. The chemical composition of subducting sediment and its consequences for the crust and mantle. Chemical Geology 145, 325–394.
Polat, A., Hofmann, A.W., 2003. Alteration and geochemical patterns in the 3.7–3.8 Ga Isua greenstone belt, West Greenland. Precambrian Research 126, 197–218.

Polderraart, A., Hess, H.H., 1951. Pyroxenes in the crystallization of basaltic magma. Journal of Geology 19, 472–489.
Powell, R., 1984. Inversion of the assimilation and fractional crystallization (AFC) equations; characterization of contaminants from isotope and trace element relationships in volcanic suites. Journal of the Geological Society, London 141, 447–452.
Putirka, K.D., 2008. Thermometers and barometers for volcanic systems. Reviews in Mineralogy and Geochemistry 69, 61–120.
Putirka, K.D., Mikaelian, H., Ryerson, F., Shaw, H., 2003. New clinopyroxene–liquid thermobarometers for mafic, evolved, and volatile-bearing lava compositions, with applications to lavas from Tibet and the Snake River Plain, Idaho. American Mineralogist 88, 1542–1554.
Qi, L., Zhou, M.F., 2008. Platinum-group elemental and Sr–Nd–Os isotopic geochemistry of Permian Emeishan flood basalts in Guizhou Province, SW China. Chemical Geology 248, 83–103.
Rudnick, R.L., Gao, S., 2003. Composition of the continental crust. In: Rudnick, R.L. (Ed.), Treatise on Geochemistry. Elsevier, Amsterdam, pp. 1–64.
Salters, V.J.M., Stracke, A., 2004. Composition of the depleted mantle. Geochemistry, Geophysics, Geosystems 5. http://dx.doi.org/10.1029/2003GC000597.
Schwandt, C.S., McKay, G.A., 2006. Minor- and trace-element sector zoning in synthetic enstatite. American Mineralogist 91, 1607–1615.
Sengör, A.M.C., Natal'In, B.A., Burtman, U.S., 1993. Evolution of the Altaid tectonic collage and Palaeozoic crustal growth in Eurasia. Nature 364, 299–307.
Shu, L.S., Wang, B., Zhu, W.B., Guo, Z.J., Charvet, J., Zhang, Y., 2011. Timing of initiation of extension in the Tianshan, based on structural, geochemical and geochronological analyses of bimodal volcanism and olistostrome in the Bogda Shan (NW China). International Journal of Earth Sciences 100, 1647–1663.
Si, G., Su, H., Yang, G., Zhang, C., Yang, G., 2014. Geological significance and geochemical characteristics of the Sikeshu pluton in North Tianshan, Xinjiang. Xinjiang Geology 32, 19–24 (in Chinese with English abstract).
Simon, A., Yogodzinski, G.M., Robertson, K., Smith, E., Selyangin, O., Kiryukhin, A., Mulcahy, S.R., Walker, J.D., 2014. Evolution and genesis of volcanic rocks from Mutnovsky Volcano, Kamchatka. Journal of Volcanology and Geothermal Research 286, 116–137.
Singer, B.S., Jicha, B.R., Leeman, W.P., Rogers, N.W., Thirlwall, M.F., Ryan, J., Nicolaysen, K.E., 2007. Along-strike trace element and isotopic variation in Aleutian Island Arc basalt: subduction melts sediments and dehydrates serpentine. Journal of Geophysical Research 112, B06206. http://dx.doi.org/10.1029/2006JB004897.
Sisson, T.W., Bronto, S., 1998. Evidence for pressure-release melting beneath magmatic arcs from basalt at Galunggung, Indonesia. Nature 391, 883–886.
Sisson, T.W., Grove, T.L., 1993a. Temperatures and H_2O contents of low-MgO high-alumina basalts. Contributions to Mineralogy and Petrology 113, 167–184.
Sisson, T.W., Grove, T.L., 1993b. Experimental investigations of the role of H_2O in calc-alkaline differentiation and subduction zone magmatism. Contributions to Mineralogy and Petrology 113, 143–166.
Stolz, A.J., Jochum, K.P., Spettel, B., Hafmann, A.W., 1996. Fluid- and melt-related enrichment in the subarc mantle: evidence from Nb/Ta variations in island-arc basalts. Geology 24, 587–590.
Sun, S.S., McDonough, W.F., 1989. Chemical and isotopic systematics of oceanic basalts: implications for mantle composition and processes. In: Saunders, A.D., Norry, M.J. (Eds.), Magmatism in the Ocean Basins. Geological Society Special Publications, pp. 313–345.
Tang, G.-J., Wang, Q., Wyman, D.A., Sun, M., Li, Z.-X., Zhao, Z.-H., Sun, W.-D., Jia, X.-H., Jiang, Z.-Q., 2010. Geochronology and geochemistry of Late Paleozoic magmatic rocks in the Lamasu-Dabata area, northwestern Tianshan (West China): evidence for a tectonic transition form arc to post-collisional setting. Lithos 119, 393–411.
Tang, G.-J., Wang, Q., Wyman, D.A., Li, Z.-X., Zhao, Z.-H., Yang, Y.-H., 2012. Late Carboniferous high εNd(t)-εHf(t) granitoids, enclaves and dikes in western Junggar, NW China: ridge-subduction-related magmatism and crustal growth. Lithos 140–141, 86–102.
Tang, G.-J., Chung, S.-L., Wang, Q., Wyman, D.A., Dan, W., Chen, H.-Y., Zhao, Z.-H., 2014. Petrogenesis of a Late Carboniferous mafic dike-granitoid association in the western Tianshan: response to the geodynamics of oceanic subduction. Lithos 202–203, 85–99.
Tilley, C.E., 1950. Some aspects of magmatic evolution. Quarterly Journal of the Geological Society of London 106, 37–50.
Tong, Y., Wang, T., Hong, D., Han, B., Zhang, J., Shi, X., Wang, C., 2010. Spatial and temporal distribution of the Carboniferous–Permian granitoids in Northern Xinjiang and its adjacement areas, and its tectonic significance. Acta Petrologica et Mineralogica 29, 619–641 (in Chinese with English abstract).
Ushioda, M., Takahashi, E., Hamada, M., Suzuki, T., 2014. Water content in arc basaltic magma in the Northeast Japan and Izu arcs: an estimate from Ca/Na partitioning between plagioclase and melt. Earth, Planets and Space 66, 127.
Vervoort, J.D., Patchett, P.J., Blichert-Toft, J., Albarede, F., 1999. Relationships between Lu–Hf and Sm–Nd isotopic systems in the global sedimentary system. Earth and Planetary Science Letters 168, 79–99.
Wang, Z.H., Sun, S., Li, J.L., Hou, Q.L., Qin, K.Z., Xiao, W.J., Hao, J., 2003. Paleozoic tectonic evolution of the Northern Xinjiang, China: geochemical and geochronological constrains from the ophiolites. Tectonics 22. http://dx.doi.org/10.1029/2002TC00139.
Wang, B.Y., Jiang, C.Y., Li, Y.J., Wu, H.E., Xia, Z.D., Lu, R.H., 2009. Geochemistry and tectonic implications of Karamaili ophiolite in east Junggar of Xinjiang. Journal of Mineralogy and Petrology 9, 74–82 (in Chinese with English abstract).
Wang, B., Shu, L., Faure, M., Jahn, B.-m., Cluzel, D., Charvet, J., Chung, S.-l., Meffre, S., 2011. Paleozoic tectonics of the southern Chinese Tianshan: insights from structural, chronological and geochemical studies of the Heiyingshan ophiolitic mélange (NW China). Tectonophysics 497, 85–104.
Wei, X., Xu, Y.-G., Feng, Y.-X., Zhao, J.-X., 2014. Plume–lithosphere interaction in the generation of the Tarim Large Igneous Province, NW China: geochronological and geochemical constraints. American Journal of Science 314, 314–356.
Wilhem, C., Windley, B.F., Stampfli, G.M., 2012. The Altaids of Central Aisa: a tectonic and evolutionary innovative review. Earth-Science Reviews 113, 303–341.
Williams, I.S., 1998. U–Th–Pb geochronology by ion microprobe. Reviews in Economic Geology 7, 1–35.
Winchester, J.A., Floyd, P.A., 1977. Geochemical discrimination of different magma series and their differentiation products using immobile elements. Chemical Geology 20, 325–343.
Windley, B.F., Allen, M.B., Zhang, C., Zhao, Z.Y., Wang, G.R., 1990. Paleozoic accretion and Cenozoic redeformation of the Chinese Tien Shan Range, Central Asia. Geology 18, 128–131.
Windley, B.F., Alexeiev, D., Xiao, W., Kröner, A., Badarch, G., 2007. Tectonic models for accretion of the Central Orogenic Belt. Journal of the Geological Society, London 164, 31–47.
Wood, D.A., 1980. The application of a Th–Hf–Ta diagram to problems of tectonomagmatic classification and to establishing the nature of crustal contamination of basaltic lavas of the British Tertiary volcanic province. Earth and Planetary Science Letters 50, 11–30.
Workman, R.K., Hart, S.R., 2005. Major and trace element composition of the depleted MORB mantle (DMM). Earth and Planetary Science Letters 231, 53–72.
Xia, L.-Q., Xia, Z.-C., Xu, X.-Y., Li, X.-M., Ma, Z.-P., Wang, L.-S., 2004. Carboniferous Tianshan igneous megaprovince and mantle plume. Geological Bulletin of China 23, 903–910 (in Chinese with English abstract).
Xia, L.-Q., Xia, Z.-C., Xu, X.-Y., Li, X.-M., Ma, Z.-P., 2008. Relative contributions of crust and mantle to the generation of the Tianshan Carboniferous rift-related basic lavas, Northwestern China. Journal of Asian Earth Sciences 31, 357–378.
Xia, L.-Q., Xu, X.-Y., Li, X.-M., Ma, Z.-P., Xia, Z.-C., 2012. Reassessment of petrogenesis of Carboniferous–Early Permian rift-related volcanic rocks in the Chinese Tianshan and its neighboring areas. Geoscience Frontiers 3, 445–471.
Xiao, L., Xu, Y.G., Mei, H.J., Zheng, Y.F., He, B., Pirajno, F., 2004a. Distinct mantle sources of low-Ti and high-Ti basalts from the western Emeishan large igneous province, SW China: implications for plume–lithosphere interaction. Earth and Planetary Science Letters 228, 525–546.
Xiao, W.-J., Zhang, L.-C., Qin, K.-Z., Sun, S., Li, J.-L., 2004b. Paleozoic accretionary and collisional tectonics of the eastern Tianshan (China): implications for the continental growth of Central Asia. American Journal of Science 304, 370–395.
Xiao, W., Han, C., Yuan, C., Sun, M., Lin, S., Chen, H., Li, Z., Li, J., Sun, S., 2008. Middle Cambrian to Permian subduction-related accretionary orogenesis of Northern Xinjiang, NW China: implications for the tectonic evolution of Central Asia. Journal of Asian Earth Sciences 32, 102–117.
Xiao, W., Windley, B.F., Allen, M.B., Han, C., 2013. Paleozoic multiple accretionary and collisional tectonics of the Chinese Tianshan orogenic collage. Gondwana Research 23, 1316–1341.
Xu, Y.G., Chung, S.L., Jahn, B.M., Wu, G.Y., 2001. Petrologic and geochemical constraints on the petrogenesis of Permian–Triassic Emeishan flood basalts in Southwestern China. Lithos 58, 145–168.
Xu, X., Li, X., Ma, Z., Xia, L., Xia, Z., Pen, G., 2006a. LA-ICPMS zircon U–Pb dating of gabbro from the Bayingou ophiolite in the northern Tianshan Mountains. Acta Geologica Sinica 80, 1168–1176 (in Chinese with English abstract).
Xu, X., Xia, L., Ma, Z., Wang, Y., Xia, Z., Li, X., Wang, L., 2006b. SHRIMP zircon U–Pb geochronology of the plagiogranites from Bayingou ophiolite in North Tianshan Mountains and the petrogenesis of the ophiolite. Acta Petrologica Sinica 22, 83–94 (in Chinese with English abstract).
Yan, Y., Xue, C., Zhang, Z., Ding, Z., Yang, W., Han, Z., 2013. Geochemistry and genesis of the Qunjisayi granite porphyry in the west of Awulale area, western Tianshan Mountains. Acta Petrologica et Mineralogica 32, 139–153 (in Chinese with English abstract).
Yang, M., Wu, H., Yang, G., 2009. Geochemical characteristics and tectonic significance of Kalameili SSZ ophiolite from Eastern Junggar. Acta Petrologica et Mineralogica 28, 251–263 (in Chinese with English abstract).
Yoder, H.S., Tilley, C.E., 1962. Origin of basalt magmas: an experimental study of natural and synthetic rock systems. Journal of Petrology 3, 342–532.
Yuan, C., Sun, M., Wilde, S., Xiao, W.J., Xu, Y.G., Long, X.P., Zhao, G.C., 2010. Postcollisional plutons in the Balikun area, East Chinese Tianshan: evolving magmatism in response to extension and slab break-off. Lithos 119, 269–288.
Zhang, C.-L., Zou, H.-B., 2013. Permian A-type granites in Tarim and western part of Central Asian Orogenic Belt (CAOB): genetically related to a common Permian mantle plume? Lithos 172–173, 47–60.
Zhang, Z.C., Mahoney, J.J., Mao, J.W., Wang, F.S., 2006. Geochemistry of picritic and associated basalt flows of the western Emeishan flood basalt province, China. Journal of Petrology 47, 1997–2019.
Zhang, W., Chen, H., Han, J., Zhao, L., Huang, J., Yang, J., Yan, X., 2015. Geochronology and geochemistry of igneous rocks in the Bailingshan area: implications for the tectonic setting of Late Paleozoic magmatism and iron skarn mineralization in the eastern tianshan, NW China. Gondwana Research http://dx.doi.org/10.1016/j.gr.2015.10.011.
Zhao, T., Xu, S., Zhu, Z., Liu, X., Chen, C., 2014. Geological and geochemical features of Carboniferous volcanic rocks in Bogda–Harlik Mountains, Xinjiang and their tectonic significance. Geological Review 60, 115–124 (in Chinese with English abstract).
Zhong, Y.-T., Xu, Y.-G., 2009. Characteristics of plume-related A-type granites: an example from the Emeishan Large Igneous Province. Journal of Jilin University (Earth Science Edition) 39, 828–838 (in Chinese with English abstract).
Zhou, M.F., Zhao, J.H., Jiang, C.Y., Gao, J.F., Wang, W., Yang, S.H., 2009. OIB-like, heterogeneous mantle sources of Permian basaltic magmatism in the western Tarim Basin,

NW China: implications for a possible Permian large igneous province. Lithos 113, 583–594.
Zhu, Y., Guo, X., Song, B., Zhang, L., Gu, L., 2009. Petrology, Sr–Nd–Hf isotopic geochemistry and zircon chronology of the Late Palaeozoic volcanic rocks in the southwestern Tianshan Moutains, Xinjiang, NW China. Journal of the Geological Society, London 166, 1085–1099.
Zimmer, M.M., Plank, T., Hauri, E.H., Yogodzinski, G.M., Stelling, P., Larsen, J., Singer, B., Jicha, B., Mandeville, C., Nye, C.J., 2010. The role of water in generating the calc-alkaline trend: new volatile data for Aleutian magmas and a new tholeiitic index. Journal of Petrology 51, 2411–2444.
Zindler, A., Hart, S., 1986. Chemial geodynamics. Annual Review of Earth and Planetary Sciences 14, 493–571.